ISSN: 2150-4091 Volume 7, Number 2, February 2015

Scientific Research Publishing

Natural Science

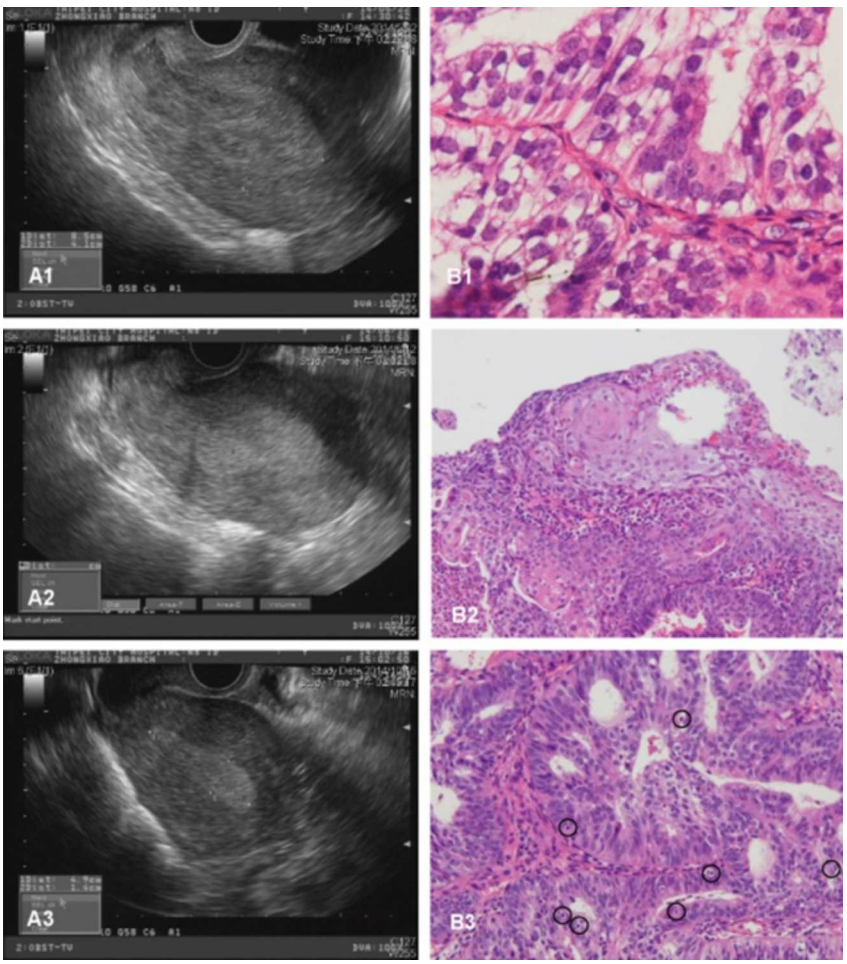

ISSN: 2150-4091

Journal Editorial Board

ISSN: 2150-4091 (Print) ISSN: 2150-4105 (Online)
http://www.scirp.org/journal/ns

Natural Science, 2015, 7, 65-102
Published Online February 2015 in SciRes. http://www.scirp.org/journal/ns

Table of Contents

Volume 7 Number 2 February 2015

The figure on the front cover is from the article published in Natural Science, 2015, Vol. 7, No. 2, pp. 71-80 by Ming Cheh Ou, *et al*.

Natural Science (NS)

Journal Information

SUBSCRIPTIONS

The *Natural Science* (Online at Scientific Research Publishing, www.SciRP.org) is published monthly by Scientific Research Publishing, Inc., USA.

Subscription rates:

Print: $89 per copy.
To subscribe, please contact Journals Subscriptions Department, E-mail: sub@scirp.org

SERVICES

Advertisements
Advertisement Sales Department, E-mail: service@scirp.org

Reprints (minimum quantity 100 copies)
Reprints Co-ordinator,Scientific Research Publishing, Inc., USA.
E-mail:sub@scirp.org

COPYRIGHT

PRODUCTION INFORMATION

For manuscripts that have been accepted for publication, please contact:
E-mail: ns@scirp.org

Natural Science, 2015, 7, 65-70
Published Online February 2015 in SciRes. http://www.scirp.org/journal/ns
http://dx.doi.org/10.4236/ns.2015.72007

Change of Receptor Binding Preference of Novel Avian Origin H7N9 in China from 2013 to 2014

Wei Hu

Department of Computer Science, Houghton College, Houghton, USA
Email: wei.hu@houghton.edu

Received 10 January 2015; accepted 28 January 2015; published 2 February 2015

Abstract

The advent of a novel avian origin H7N9 emerged in China in March 2013 is of major health concern, as it has little virulence in birds but can cause severe illness and death in humans. As people continue to get infected by this new virus in 2014, we need to understand the current status and trend of its evolution at the end of year 2014. The influenza viruses have two surface proteins, haemagglutinin (HA) and neuraminidase (NA), which are involved in viral entry into and egress from the host cells respectively. In a previous study published in May 2013, we found that the HA protein of this new human H7N9 virus was able to preferentially bind to the avian type receptors as its primary binding and human type receptors as its secondary, which was confirmed by several web lab experiments a few months later in 2013. The current study examined the binding preference of human H7N9 again trying to uncover any change in the HA binding properties as this virus ran its course from 2013 to 2014. Our analysis concluded that the HA binding patterns of this novel virus were stable and similar to avian H7N9 in Asia and in Europe until August 2013, but after that time the virus gradually started to change and exhibit enhanced binding features of avian H7N9 in North America. Further investigation of the observed change identified a few positions in HA that could be potentially important for distinguishing the HA sequences of human H7N9 in China collected before and after August 2013. As a result, we discovered a single amino acid substitution R47K in HA that was believed to be the primary cause for this shift of binding patterns. Finally, our findings also implied that the human infections with H7N9 in China in 2013 were more likely caused by chickens than by ducks.

Keywords

H7N9, Influenza, Receptor Binding Specificity, HA Gene

How to cite this paper: Hu, W. (2015) Change of Receptor Binding Preference of Novel Avian Origin H7N9 in China from 2013 to 2014. *Natural Science*, **7**, 65-70. http://dx.doi.org/10.4236/ns.2015.72007

1. Introduction

The emergence of new influenza viruses is a constant public health concern. In March 2013, a novel avian origin H7N9 virus was discovered in China that can infect humans and cause death. This novel H7N9 strain is the first H7 subtype discovered in Asia that is transmittable from birds to humans. A typical pathway of such infection is from migratory birds to domestic ducks, to chickens, then possibly to humans. In general, however, avian H7N9 is considered as low pathogenic, which makes it difficult for detection and control as birds infected by this virus may show no symptom at all. The World Health Organization updated as of 21 November 2014 that from 14 to 20 November 2014, 3 new cases of human H7H9 infection were reported from China in the western pacific region [1]. The fact that people in China continue to get infected by this new virus raises concerns about its ability to transmit in the human population and reminds us of the urgent need to know what is happening inside this virus today.

The eight gene segments of this new human H7N9 virus come from different avianinfluenza viruses through a sequence of events that could have involved mixing between wild and domestic ducks and reassortment in poultry. Two of the glycoproteins comprising the exterior structure of influenza viruses are haemagglutinin (HA) and neuraminidase (NA). Further, the HA protein has two subunits: HA1 subunit (globular head domain) and HA2 subunit (stem domain).

The HA protein is involved in the initial viral attachment and binding to a host cell. After infection the virus uses the host cell's reproduction machinery to multiply and eventually exit the cell through the help of NA protein which results in death of the host cell. The functions of these two proteins are complementary, *i.e.*, the HA protein is to bind receptors on a host cell whereas NA is to destroy the receptors to enable progeny escape from the infected cell. Thus, a balance between HA and NA needs to be maintained. Moreover, an overactive NA activity could be detrimental to virus survival by destroying receptors on uninfected cells necessary for HA to bind.

The receptor binding affinity of a virus can determine what host can be infected because the first step of influenza infection is HA binding to receptors found on the host cell surface. Receptor binding properties are also critical for pathogenicity. One of the biological traits required for avian viruses to cross the species barrier to infect humans is the change of their HA binding preference. Avian and human viruses typically have a different receptor binding preference and only few amino acid changes in the HA protein could cause a switch from avian to human receptor specificity. This difference in receptor binding accounts for the reduced ability of avian strains to establish infections in humans.

The HA gene of human H7N9 is related to avian H7N3 viruses circulating in China prior to 2013, while the NA protein is similar to that of avian H11N9 and H2N9 from migratory birds, both of which are derived from the Eurasian lineage of avian viruses [2] [3]. We evaluated the HA binding of this new virus right after its advent in China in March 2013. Our findings published in May 2013 [4] suggested that the primary binding avidity of this virus is to avian types of receptors and its secondary binding is to human types, which were later verified by several wet lab experiments using glycan arrays, virus histochemistry, animal models, and structural analyses of HA [5]-[11].

The interesting part of the work in [7] is that they noticed a subtle difference in HA binding studies using a whole virus or just the HA protein alone, as the HA binding is influenced by the NA protein, which preferentially cleaves avian type receptors. Having dual binding to human and avian type receptors makes the new H7N9 virus different from avian H5N1, which bounds more strongly to avian receptors. This may be one reason why this virus is able to cause so many human infections quickly.

The purpose of the current study was to apply the methodology developed in [4] [12] [13] to examine any change in the HA binding of human H7N9 in China when it ran its course of evolution and adaptation in human population from 2013 to 2014.

2. Materials and Methods

2.1. Sequence Data

We downloaded the HA protein sequences of human and avian H7N9 in China and other regions from the Global Initiative on Sharing Avian Influenza Data (GISAID) database (http://platform.gisaid.org).

2.2. Informational Spectrum Method

The informational spectrum method (ISM) is a bioinformatics approach to analyze protein sequences [3] [4] [12]. The main idea of this method is to apply Discrete Fourier Transform (DFT) to protein sequences that are represented as letters for amino acids. Therefore, before DFT can be used the protein sequences have to be transformed into numerical sequences based on electron-ion interaction potential (EIIP) of each amino acid. Then the resulting DFT coefficients are employed to produce the energy density spectrum. The informational spectrum (IS) comprises the frequencies and the amplitudes of this energy density spectrum. According to the ISM theory, the peak frequencies of IS of a protein sequence reflect its biological or biochemical functions. The ISM was successfully applied to quantify the effects of HA mutations on the receptor binding preference in [14] [16].

In [14] [15] ISM was applied to study the novel H7N9 of avian origin in China in 2013, which discovered that the primary IS frequency is F(0.285) for avian receptor binding and the secondary is F(0.326) for human receptor binding. We also demonstrated that human H7N9 and avian H7N9 in China in 2013 share the same HA receptor binding properties. Furthermore, mutations that could alter the HA binding preference of this new virus were also found and analyzed.

3. Results

The present study aimed to investigate the possible change in HA binding affinity of human H7N9 as it ran its course from 2013 to 2014. In order to shed light on any change in the receptor binding specificity of human H7N9 in China from 2013 to 2014, we compared this virus with its avian counterpart: avian H7N9 in Asia (chicken and duck), avian H7N9 in Europe, and in North America. First, the IS amplitudes at top four frequencies of human H7N9 in China were plotted in order of their collection dates (**Figure 1**), though not every sequence had a collection date or even a month in our whole dataset.

Our ISM analysis clearly indicated that these four IS amplitudes of human H7N9 in China remained stable until August 2013, after which they started to oscillate. The third and fourth IS amplitudes were increasing after August 2013 with the third increased more than the fourth. To investigate the meaning of this frequency F(0.166), we included HAs from avian H7N9 from different continents. It turned out that F(0.166) was the primary IS frequency for avian H7N9 in North America. For chicken HA sequences in Asia, we only had those from China, with none from other Asian countries. Unfortunately we did not have the chicken HA sequences in China after July 1 2013. Otherwise it would be interesting to see any HA binding changes in chicken population after this time.

It is commonly believed that a typical infection pathway of avian influenza viruses is from wild aquatic birds to domestic ducks, to chickens, and then maybe finally to humans. We analyzed the HAs of avian H7N9 in Asia grouped by duck and chicken, which demonstrated that the HA bindings of chicken H7N9 in Asia were closer to human H7N9 in China emerged in 2013 than to duck H7N9 in Asia (**Figure 1**). This also implied that the source of human infections with H7N9 in China in 2013 was more likely from chickens than from ducks. Further, the HA binding properties of avian H7N9 in Asia are closer to those in Europe than in North America (**Figure 1**).

To reveal any amino acid change in HA1 that might cause the observed change in HA binding of human H7N9 in China, we used Random Forest to find the important residues in HA that were critical for differentiating the HA1 sequences between before and after August 2013 (**Figure 2**). Next we wanted to find out, among these positions in HA1, any amino acid substitutions capable of enhancing the HA binding of human H7N9 at F(0.166). One consensus sequence was generated for the HA sequences before August 2013 and one for those after. Surprisingly, these two consensus sequences only differed in HA1 at residue 47 with the first consensus carrying 47R and the second 47K. The IS plots of these two consensus sequences demonstrated that the substitution R47K could increase the IS amplitude of human H7N9 at F(0.166) (**Figure 3**), the primary binding frequency of avian H7N9 in North America (**Figure 1**). Further sequence examination showed that the HA sequences of both avian H7N9 in Europe and in North America carried47R, and the first collected HA sequence containing 47K in avian H7N9 in Asia was A/wild bird/Korea/A3/11 (H7N9), suggesting the substitution R47K was a feature of H7N9 in Asia.

4. Conclusions

The novel human H7N9 discovered in March 2013 in China continue to infect people in 2014. Compared to

Figure 1. IS of human and avian H7N9 in difference regions (All the sequences were ordered by collection dates. However, not all the sequences had a collection date, so some of them only had year or year and month).

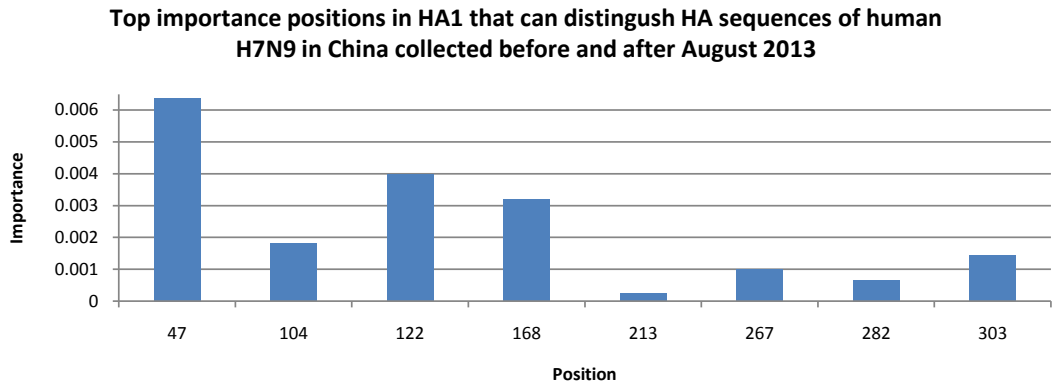

Figure 2. Top important positions in HA1 that could be used to differentiate the HA sequences of human H7N9 in China collected before and after August 2013.

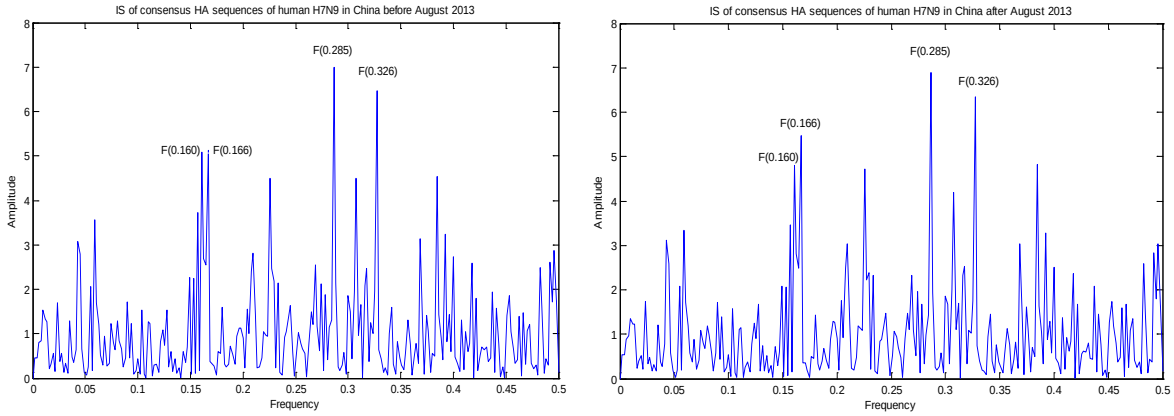

Figure 3. IS of consensus HA sequences of human H7N9 in China before or after August 2013 to show the impact of substitution R47K on the IS at F(0.166) as the two consensuses differed only at residue 47.

other avian influenza viruses, this H7N9 virus exhibits its ability to transmit from birds to humans more readily. This new virus shows low pathogenicity in birds but human infections can be deadly. Thus, it is of great importance to understand the extent to which the current H7N9 virus has evolved to acquire capabilities for transmission among humans. The HA protein allows influenza viruses to attach to receptors on host cells. After they get inside and replicate, the NA protein helps the new viruses to exit and find new cells to infect. Therefore, the receptor binding preference of HA is critical for viral replication and transmission.

The change of binding specificity from avian type receptors to human type receptors is thought to be a prerequisite for an avian virus to infect humans. The human H7N9 virus has dual binding to avian and human receptors, which makes it more readily to infect humans than other avian strains such as H5N1. This study took a closer look at this virus at the end of year 2014, more specifically its HA receptor binding preference. Our analysis revealed that the HA binding patterns of human H7N9 were stable and similar to its counterparts, avian H7N9 in Asian and in Europe, from March 2013 to August 2013, but after August 2013, they started to oscillate and exhibit enhanced binding patterns of avian H7N9 in North America. The uncovered change in the HA binding properties of this new virus was further explored by identification of the important resides in HA to differentiate the HA sequences of this virus collected before August 2013 and after. As a result, a single amino acid substitution R47K in HA was identified that might be responsible for this change in HA binding properties of human H7N9. We also found that the HA binding patterns of human H7N9 were closer to chicken H7N9 than to duck H7N9 in China.

Acknowledgements

We thank Houghton College for its financial support.

References

[1] http://www.wpro.who.int/outbreaks_emergencies/H7N9/en/

[2] Neumann, G., Macken, C.A. and Kawaoka, Y. (2014) Identification of Amino Acid Changes That May Have Been Critical for the Genesis of A(H7N9) Influenza Viruses. *Journal of Virology*, **88**, 4877-4896. http://dx.doi.org/10.1128/JVI.00107-14

[3] Liu, D., Shi, W., Shi, Y., Wang, D., Xiao, H., Li, W., Bi, Y., Wu, Y., Li, X., Yan, J., Liu, W., Zhao, G., Yang, W., Wang, Y., Ma, J., Shu, Y., Lei, F. and Gao, G.F. (2013) Origin and Diversity of Novel Avian Influenza A H7N9 Viruses Causing Human Infection: Phylogenetic, Structural, and Coalescent Analyses. *Lancet*, **381**, 1926-1932. http://dx.doi.org/10.1016/S0140-6736(13)60938-1

[4] Hu, W. (2013) Receptor Binding Specificity and Sequence Comparison of a Novel Avian-Origin H7N9 Virus in China. *Journal of Biomedical Science and Engineering*, **6**, 533-542. http://dx.doi.org/10.4236/jbise.2013.65068

[5] Shi, Y., Zhang, W., Wang, F., Qi, J., Wu, Y., Song, H., Gao, F., Bi, Y., Zhang, Y., Fan, Z., Qin, C., Sun, H., Liu, J., Haywood, J., Liu, W., Gong, W., Wang, D., Shu, Y., Wang, Y., Yan, J. and Gao, G.F. (2013) Structures and Receptor Binding of Hemagglutinins from Human-Infecting H7N9 Influenza Viruses. *Science*, **342**, 243-247. http://dx.doi.org/10.1126/science.1242917

[6] Xiong, X., Martin, S.R., Haire, L.F., Wharton, S.A., Daniels, R.S., Bennett, M.S., McCauley, J.W., Collins, P.J., Walker, P.A., Skehel, J.J. and Gamblin, S.J. (2013) Receptor Binding by an H7N9 Influenza Virus from Humans. *Nature*, **499**, 496-499. http://dx.doi.org/10.1038/nature12372

[7] Xu, R., de Vries, R.P., Zhu, X., Nycholat, C.M., McBride, R., Yu, W., Paulson, J.C. and Wilson, I.A. (2013) Preferential Recognition of Avian-Like Receptors in Human Influenza A H7N9 Viruses. *Science*, **342**, 1230-1235. http://dx.doi.org/10.1126/science.1243761

[8] Zhu, H., Wang, D., Kelvin, D.J., Li, L., Zheng, Z., Yoon, S.W., Wong, S.S., Farooqui, A., Wang, J., Banner, D., Chen, R., Zheng, R., Zhou, J., Zhang, Y., Hong, W., Dong, W., Cai, Q., Roehrl, M.H., Huang, S.S., Kelvin, A.A., Yao, T., Zhou, B., Chen, X., Leung, G.M., Poon, L.L., Webster, R.G., Webby, R.J., Peiris, J.S., Guan, Y. and Shu, Y. (2013) Infectivity, Transmission, and Pathology of Human H7N9 Influenza in Ferrets and Pigs. *Science*, **341**, 183-186. http://dx.doi.org/10.1126/science.1239844

[9] Watanabe, T., Kiso, M., Fukuyama, S., Nakajima, N., Imai, M., Yamada, S., Murakami, S., *et al*. (2013) Characterization of H7N9 Influenza A Viruses Isolated from Humans. *Nature*, **501**, 551-555. http://dx.doi.org/10.1038/nature12392

[10] Belser, J.A., Gustin, K.M., Pearce, M.B., Maines, T.R., Zeng, H., Pappas, C., Sun, X., Carney, P.J., Villanueva, J.M., Stevens, J., Katz, J.M. and Tumpey, T.M. (2013) Pathogenesis and Transmission of Avian Influenza A (H7N9) Virus in Ferrets and Mice. *Nature*, **501**, 556-559. http://dx.doi.org/10.1038/nature12391

[11] Ramos, I., Krammer, F., Hai, R., Aguilera, D., Bernal-Rubio, D., Steel, J., García-Sastre, A. and Fernandez-Sesma, A. (2013) H7N9 Influenza Viruses Interact Preferentially with α2, 3-Linked Sialic Acids and Bind Weakly to α2, 6-Linked Sialic Acids. *Journal of General Virology*, **94**, 2417-2423. http://dx.doi.org/10.1099/vir.0.056184-0

[12] Hu, W. (2013) Mutations in Hemagglutinin of a Novel Avian-Origin H7N9 Virus That Are Critical for Receptor Binding Specificity. *Tsinghua Science and Technology*, **18**, 522-529. http://dx.doi.org/10.1109/TST.2013.6616525

[13] W. Hu (2014) Functional Interplay between Hemagglutinin and Neuraminidase of Pandemic 2009 H1N1 from the Perspective of Virus Evolution. *Lecture Notes in Computer Science*, **8492**, 38-49.

[14] Cosic, I. (1997) The Resonant Recognition Model of Macromolecular Bioreactivity, Theory and Application. Birkhauser Verlag, Berlin.

[15] Veljkovic, V., Niman, H.L., Glisic, S., *et al*. (2009) Identification of Hemag-Glutinin Structural Domain and Polymorphisms Which May Modulate Swine H1N1 Interactions with Human Receptor. *BMC Structural Biology*, **9**, 62. http://dx.doi.org/10.1186/1472-6807-9-62

[16] Veljkovic, V., Veljkovic, N., Muller, C.P., *et al*. (2009) Characterization of Conserved Properties of Hemagglutinin of H5N1 and Human Influenza Viruses: Possible Consequences for Therapy and Infection Control. *BMC Structural Biology*, **7**, 9-21.

Natural Science, 2015, 7, 71-80
Published Online February 2015 in SciRes. http://www.scirp.org/journal/ns
http://dx.doi.org/10.4236/ns.2015.72008

The Preliminary Approach for the Human Cancer Regression by the Interaction between Human Bilateral Symmetrical Parts—Ou MC Decrescendo Phenomenon

Ming Cheh Ou[1,2*], Dennis Ou[3], Chung Chu Pang[4]

[1]Department of Obstetrics and Gynecology, Taipei City Hospital, Taipei City, Taiwan
[2]Department of Obstetrics and Gynecology, Taipei Medical University, Taipei City, Taiwan
[3]Department of Mechanical Engineering and Biomedical Engineering, Carnegie Mellon University, Pittsburgh, USA
[4]Department of Obstetrics and Gynecology, Su Women Hospital, Taipei City, Taiwan
Email: [*]mcou@ym.edu.tw

Received 20 January 2015; accepted 10 February 2015; published 11 February 2015

Abstract

Ou MC decrescendo phenomenon (OuDP) is induced by interaction between human bilateral features and has shown to alleviate or cure infectious and non-infectious diseases. The resolution of non-infectious conditions with OuDP indicates to be consistent with restoration of normal tissue function (AJEM, 2012; Proc Physiol Soc, 2014). Ou MC handing remedy (HR) was utilized to induce OuDP by applying the hand to the contralateral body. Four female patients received self-administered HR separately for their diseases: 1) uterine endometrioid carcinoma stage IIIB, 2) suspicious pancreatic cancer in stage IA with isodense pancreatic nodule, elevated CA199 and dilated tortuous main pancreatic duct, 3) uterine leiomyosarcoma stage IB, and 4) suspicious gluteal metastatic lesion of chronic myelogenous leukemia. The treatments with HR showed to suppress or ameliorate oncologic changes for these patients: 1) The uterine endometrioid carcinoma regressed from stage IIIB to IA with 5 months treatment. 2) The pancreatic isodense lesion decreased from 1.6 × 1.7 to 1.0 × 1.0 cm in size with CA199 descending from 1090.0 to 136.5 (Unit/ml) associating with the main pancreatic duct diameter decreasing from 0.39 to 0.14 cm with tortuosity disappearance after 4 months treatment. 3) The frequent profuse bleeding by uterine leiomyosarcoma prominently decreased immediately with HR and subsequent HR was also effective at minimizing heavy uterine bleeding in the 3 weeks treatment. 4) The gluteal macular lesion of the case with chronic myelogenous leukemia was eliminated with 2 weeks treatment. It reveals OuDP may normalize the tumor cells and microenvironment function, which makes tumor cells conform to the

[*]Corresponding author.

How to cite this paper: Ou, M.C., Ou, D. and Pang, C.C. (2015) The Preliminary Approach for the Human Cancer Regression by the Interaction between Human Bilateral Symmetrical Parts—Ou MC Decrescendo Phenomenon. *Natural Science*, **7**, 71-80. http://dx.doi.org/10.4236/ns.2015.72008

regulations with apoptosis, metastasis suppression, preventing uninhibited proliferation, minimizing angiogenesis and supervision by host immunological systems. These findings warrant further investigation.

Keywords

Cancer Regression, Ou MC Decrescendo Phenomenon, Normalization of Tissue Function, Microenvironment, Apoptosis

1. Introduction

Our knowledge of cancer biology has led to many frontiers of cancer prevention, early detection, and treatment; nonetheless, modern cancer treatment is yet inefficient in comparison to other specific managements for example, antibiotics for infectious diseases [1] [2]. If cancer metastasis occurs, conventional cancer treatments as surgery, chemotherapy, and radiation therapy are generally incompetent and may eventually lead to patient death with severe complications. Recently-developed targeted treatments such as growth-signal inhibition, angiogenesis inhibition, and apoptosis induction pose fewer complications than conventional cancer treatments. Nonetheless, targeted cancer treatments may fail for targeted therapeutic agents usually inhibit key pathways in a tumor but can not completely cease malignant behavior of tumors or the resistance to targeted therapeutic agents may develop with tumor cells [2] [3]. Hormonal or biological response modifiers treatments also cause fewer side effects but also usually become ineffective if cancer resistance evolves [4] [5]. More frontiers against cancer are indicated to improve the capacity for cancer treatment.

The formation of a clinically-relevant tumor requires support from the surrounding stroma which also is referred to as the tumor microenvironment. Recent studies show that bidirectional interaction between tumor cells and microenvironment is essential for oncogenesis, tumor growth, and metastasis. Thus, many cellular and molecular elements of the tumor microenvironment are emerging as attractive targets for therapeutic strategies [6]. The way to normalize tumor microenvironment may be helpful to suppress tumor growth or extirpate cancer cells.

Ou MC decrescendo phenomenon (OuDP) is induced by the interaction between human bilateral symmetrical features [7] [8]. It has shown to be capable of normalizing tissue function, which has caused resolution of joint pain, soft tissue edema, constipation and organ dysfunction in recent studies. OuDP has also shown to be effective for patients with warts through long-term treatment [9] [10]. In this study, we further observe the effect of OuDP on cancer.

2. Methods

2.1. Subjects

From 2011 to 2014, four female patients separately with uterine endometrioid carcinoma, pancreatic isodense lesion, uterine leiomyosarcoma, and chronic myelogenous leukemia (CML) with gluteal macular cutaneous lesion performed self-administered HR (**Table 1**). The case with uterine leiomyosarcoma was treated with oral ergonovine maleate (Johnson Chemical, New Taipei City, Taiwan) and tranexamic acid (Standard Chem & Pharm, Tainan, Taiwan) for the initial 5 days of the 3 weeks HR treatment while the patient with CML was treated with Glivec (Novaris, East Hanover, NJ, USA). These 2 cases were reported in a previous study and were included for an in-depth observation of OuDP's effect on human cancer [9]. The other 2 patients have not received other treatments.

2.2. Ou MC Decrescendo Phenomenon Technique

Ou MC handing remedy (HR) was performed to induce OuDP. The performance of HR is shown in **Figure 1** and **Table 2**. The patient or therapist places the contralateral hand directly on the affected area (**Figure 1**). No further hand movement is required. For lesions on or adjoining the midline of the body, the HR is applied to one side of the lesion then to the other (**Figure 1(B1-B3)**). The amount of pressure is commensurate with the depth of the lesion (**Figure 1(C1-C3)**). Multiple fingers or the back of hand can be used if the palm cannot reach

Table 1. The effect of Ou MC decrescendo phenomenon[a].

Case	Disease	Age	Diagnosis	Ou MC handing remedy (HR)		Short term effect	Long term effect
				Duration	Method		
1	Uterine endometrioid cancer, stage IIIB	49	Pathology	5 months	Press hand on bilateral lower abdomen and perineum in first 2 months; then, press hand deeply into bilateral pelvis and press hand on bilateral perineum and whole abdomen occasionally.	Heavy uterine bleeding diminishing to trace and never recurred up to date.	a. Slow tumor regression for first 2 months. b. Stage IIIB regressing to stage IA in the next 3 months.
2	Suspicious pancreatic cancer IA with isodense lesion in pancreatic tail	51	Radiology	4 months	Press hand deeply into epigastric area bilaterally and occasionally on bilateral costovertebral angles and whole abdomen.	Not observed.	a. Lesion size decreasing from 1.6 × 1.7 to 1.0 × 1.0 cm. b. Main pancreatic duct diameter decreasing from 0.39 cm to 0.14 cm. c. CA 199 descending from 1090 to 136.5 (Unit/ml). CA 125 from 50.2 to 25.4 (Unit/ml).
3	Uterine leiomyosarcoma, stage IB	59	Pathology	3 weeks	Press hand on bilateral lower abdomen.	Stopping active uterine bleeding immediately.	Trace uterine bleeding with following HR.
4	Perineal macular lesion with CML	39	Inspection	2 weeks	Place finger directly on the lesion.	Not observed.	Lesion resolved.

[a]Ou decrescendo phenomenon is induced by Ou MC handing remedy; CML, chronic myelogenous leukemia.

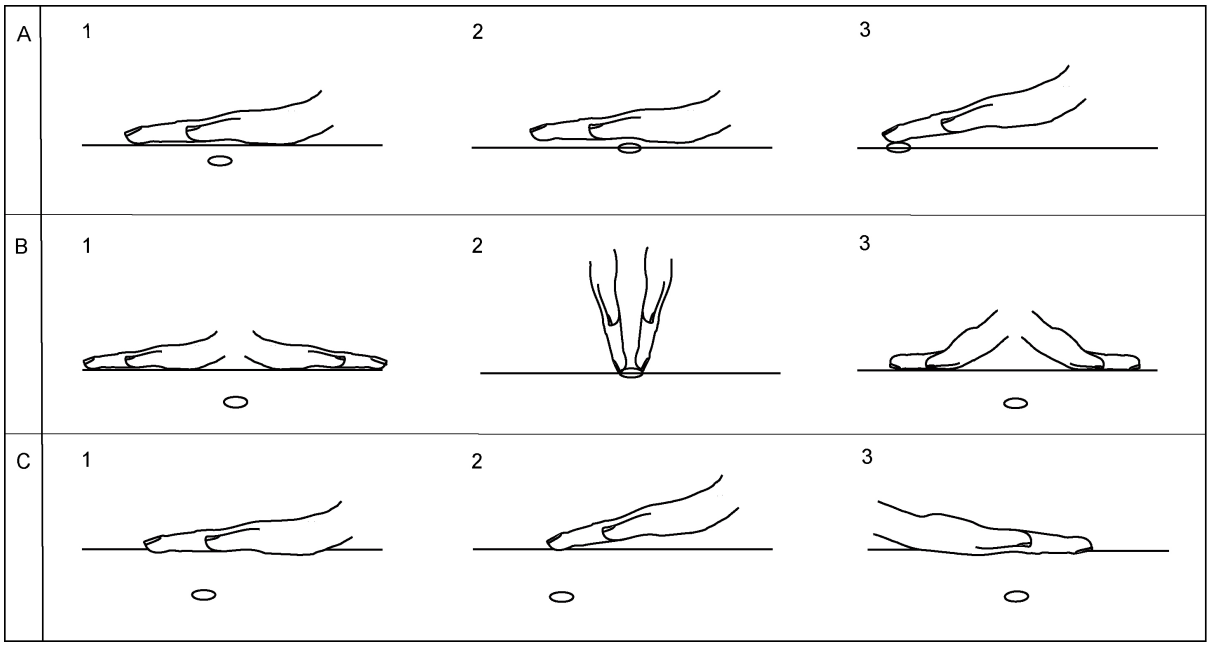

Figure 1. Schematic of the Ou MC handing remedy (HR) technique. The HR was performed by placing the contralateral hand on the affected area (A1-A3). For lesions on or adjoining the midline of the body, the HR is applied to one side of the lesion then to the other (B1-B3). The amount of pressure is commensurate with the depth of the lesion (C1-C3). Multiple fingers or the back of hand can be used if the palm cannot reach the affected area (A3-C3). For skin lesions, the palm may be kept about 0.5 cm over the lesion without touching the skin (A2). ⬭ = lesion. (From Ou MC *et al*. 2014; Ref. [9] [10]).

the affected area (**Figure 1(A3)**, **Figure 1(B3)**, and **Figure 1(C3)**). For skin lesions, the palm may be kept approximately 0.5 cm above the lesion without touching the skin (**Figure 1(A2)**), which is detailed in **Table 2** [9] [10]. All the patients were trained to administer HR by themselves.

2.3. Informed Consent

Though complementary therapy is exempt from informed consent by the law in Taiwan [11], all patients provided consent for participation in this study.

3. Results

3.1. Uterine Endometrioid Carcinoma Stage IIIB

3.1.1. Disease

This 49-year-old woman had recurrent menorrhagia and metrorrhagia for 5 years before HR treatment which has been performed from May 16, 2014 and this patient was followed up to November 4, 2014. On the night of May 15, 2014, she had profuse vaginal bleeding and received uterine dilatation and curettage (D & C). During D & C, a brownish tumor mass about 3 cm protruded from the cervical os and could not be removed by curettage. Biopsies of the cervical tumor and curettage of uterine cavity were performed. Pathology of both cervical biopsies and endometrium observed with an Olympus light microscopy (BX-51, Olympus, Tokyo, Japan) showed grade 1 endometrioid carcinoma (**Figure 3(B1)**) with negative for P16 (CINtec® Histology Kit, Ventana Medical Systems, Tuscon, AZ, USA), positive for vimentin (monoclonal mouse anti-vimentin, clone V9, DAKO, Glostrup, Denmark), estrogen receptor (estrogen receptor liquid mouse monoclonal antibody, NCL-L-ER-6F11, Newcastle, United Kingdom) and progesterone receptor (monoclonal mouse anti-human progesterone receptor, clone PgR 636, DAKO, Glostrup, Denmark). No definite squamous metaplasia or apoptosis-like lesion can be identified. Tumor markers as AFP, CEA, CA125, CA153, CA 199, and ferritin (Electro-chemiluminescence immunoassay, Elecsys, Roche Diagnostics GmbH, Mannheim, Germany), showed normal values.

3.1.2. HR Treatment

The patient refused medical or surgical treatment for unknown reason and began to perform HR since the next morning after D & C by pressing her hands on the lower abdomen and perineal area for 1 - 2 minutes, 2 times a day (**Figure 1(C1)**, **Figure 1(C2)**). Immediately, the vaginal bleeding rapidly decreased to a minimum with occasional spotting up to date. Computed tomography scan (CT) on May 18 showed a uterine tumor with suspicious myometrial penetration through the posterior wall of uterus (**Figure 2(A1)**, **Figure 2(A2)**). Sonography on May 22 showed intrauterine mass about 8.5 cm in long axis and 4.1 cm in thickness with cervical involvement (**Figure 3(A1)**). The cervical protruding tumor shrank to approximately 1 cm in diameter on May 29 and disappeared on June 12. Another endometrial biopsy was performed on June 12 and showed tumor cells with prominent squamous metaplasia and apoptosis-like changes (**Figure 3(B2)**, **Figure 3(B3)**). Sonography on June 12 showed the tumor continuously regressing (**Figure 3(A2)**). Nonetheless, MRI (Magnetic resonance imaging) on July 14 showed the size of intrauterine lesion about 8.7 × 4.9 × 3.2 cm (long axis × transverse × thickness) with parametrial invasion and penetrating through posterior uterine wall with rectal involvement (**Figure 2(B1)**, **Figure 2(B2)**). A uterine endometrioid carcinoma stage IIIB (T3N0M1) was diagnosed for this patient.

Table 2. Practical points for the application of self-administered Ou MC handing remedy (HR).

1.	The HR is performed by the patients themselves by placing the contralateral hand directly on the affected area according to Ou MC decrescendo phenomenon (**Figure 1**).
2.	For lesions on or adjoining the midline of the body, the HR is applied first to one side of the lesion and then the other.
3.	The effects of Ou MC decrescendo phenomenon are related to the duration, frequency of administration and the distance between the hand and the lesion.
4.	If HR is not efficacious, measures such as getting the hand nearer to the lesion, applying other hand gesture and increasing the duration or frequency of administration may be helpful[a].
5.	Patient positioning may be useful when performing the HR. For example, when treating lumbosacral pain, the patient may wish to lie down (supine) with the contralateral hand beneath the affected lumbosacral and adjoining areas.
6.	Severe emotional disturbance possibly may affect HR's effectiveness[b].

[a]The effect or appropriate duration and frequency of HR treatment for various diseases requires further study. [b]Whether emotional disturbance affects the efficacy of the Ou MC decrescendo phenomenon is not explored in the present study (From Ou MC *et al*., 2014; Ref. [9] [10]).

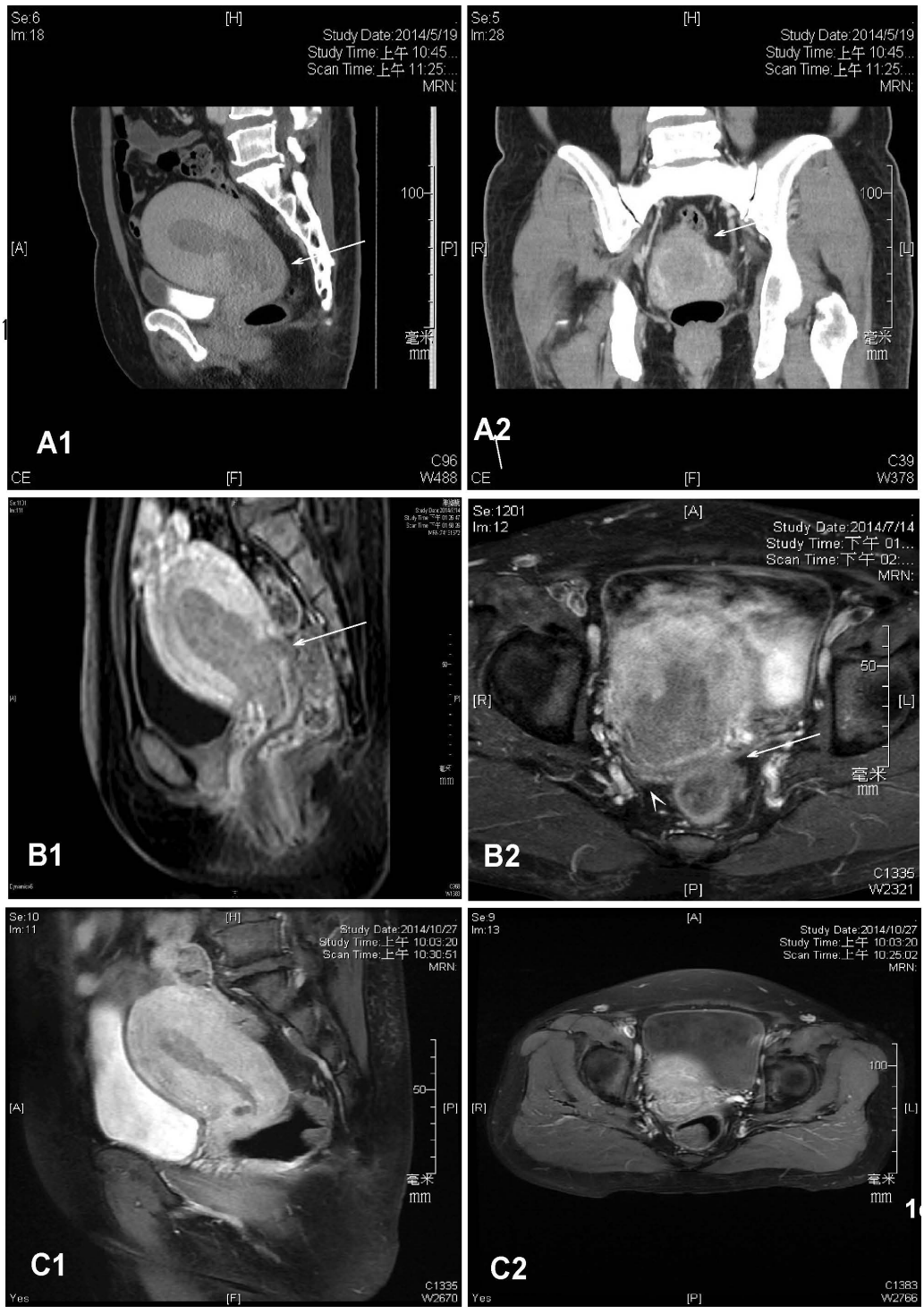

Figure 2. Uterine endometrioid carcinoma of case 1. (A) CT scan image on May 19, 2014. A1: the tumor involved uterine cavity and cervix with suspicious posterior uterine wall invasion (arrow). A2: the tumor with suspicious involvement of whole layer of posterior uterine wall (arrow). (B) MRI on July 14, 2014. B1: the lesion in uterine cavity about 8.9 × 4.9 × 4.5 cm (long axis × transverse × thickness) with posterior uterine wall invasion into the pelvis (arrow). B2: uterine parametrial invasion (arrow head) and posterior wall involvement with loss of the fat layer between uterine cervix and rectum (arrow). (C) MRI on October 27, 2014. C1: no posterior wall involvement and the lesion confined in uterine cavity about 6.7 × 3.2 ×1.5 cm. C2: uterine cervix with no tumor. CT scan, Computed tomography; MRI, Magnetic resonance imaging.

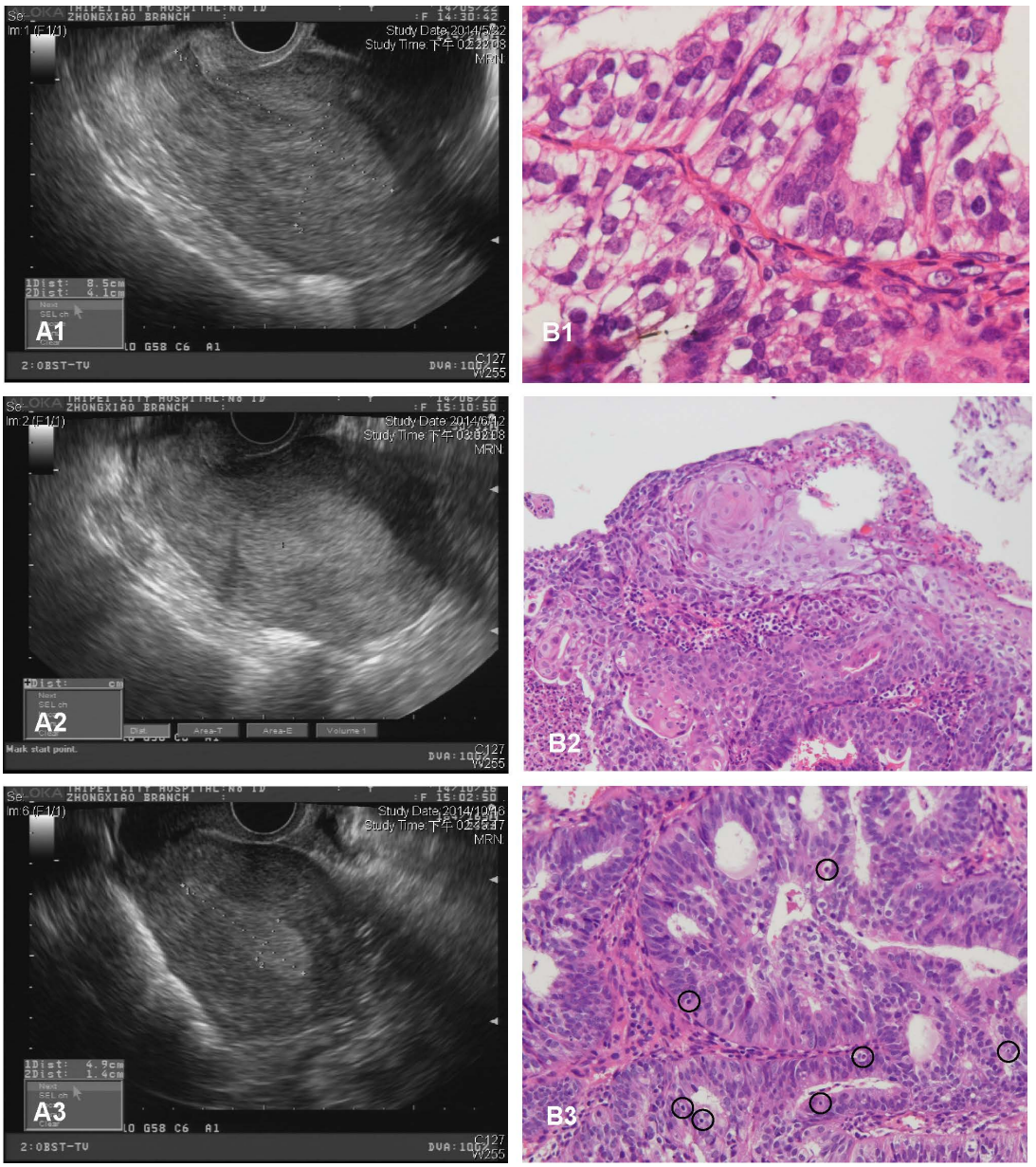

Figure 3. Uterine endometrioid carcinoma of case 1. (A) Sonography in 2014 on May 22 (A1), June 12 (A2) and October 16 (A3) showed continuous size reduction of the tumor. (B) Endometrial biopsy (hematoxylin and eosin staining, 3008-3, 3204-3, Muto Pure Chemical, Tokyo, Japan). (B1) Biopsy on May 15, 2014 showed well differentiated endometrioid carcinoma with secretory vacuoles. (magnification 400×). (B2) Biopsy on June 12, 2014 showed prominent squamous metaplasia of tumor cells (magnification 100×). (B3) Biopsy on June 12, 2014 showed numerous apoptosis-like cells (black circle, magnification 100×).

3.1.3. Reinforced HR Treatment

Thus, the patient began to reinforce HR treatment by placing her hand deeply into the bilateral pelvic region for 2 minutes on each side of uterus in the morning and 10 minutes at night (**Figure 1(C1)**, **Figure 1(C2)**). She also placed her hand on the contralateral perineal area or other abdominal areas if experiencing abdominal fullness (**Figure 1(C1)**, **Figure 1(C2)**). Sonography on October 16 showed an intrauterine mass about 4.9 × 1.8 × 1.4 cm with no cervical involvement (**Figure 3(A3)**). MRI on October 27 showed intrauterine mass about 6.7 × 3.2 × 1.5 with no cervical, parametrial or pelvic involvement (T1N0M0, Stage IA, **Figure 2(C1)**, **Figure 2(C2)**); however, this patient refused endometrial biopsy on November 4.

3.2. Suspicious Pancreatic Cancer IA with Elevated CA199 and Dilated Tortuous Main Pancreatic Duct

3.2.1. Disease

This 51-year-old patient was discovered with CA-199 of 67.1 (Unit/ml) (normal <27) and CA125 of 31 (Unit/ml) (normal <35) on March 13, 2014. She was followed up to October 21, 2014. CA 199 of 1090.0 and CA125 of 46.5 were found for her on May 26. The CT scan examination she received on May 29 showed an isodense nodule about 1.6 × 1.7 cm in greatest dimension (**Figure 4(A1)**, **Figure 4(A2)**) in the pancreatic tail with dilated tortuous main pancreatic duct in a diameter about 0.39 cm (**Figure 4(A3)**). A pancreatic cancer, stage IA was tentatively presumed.

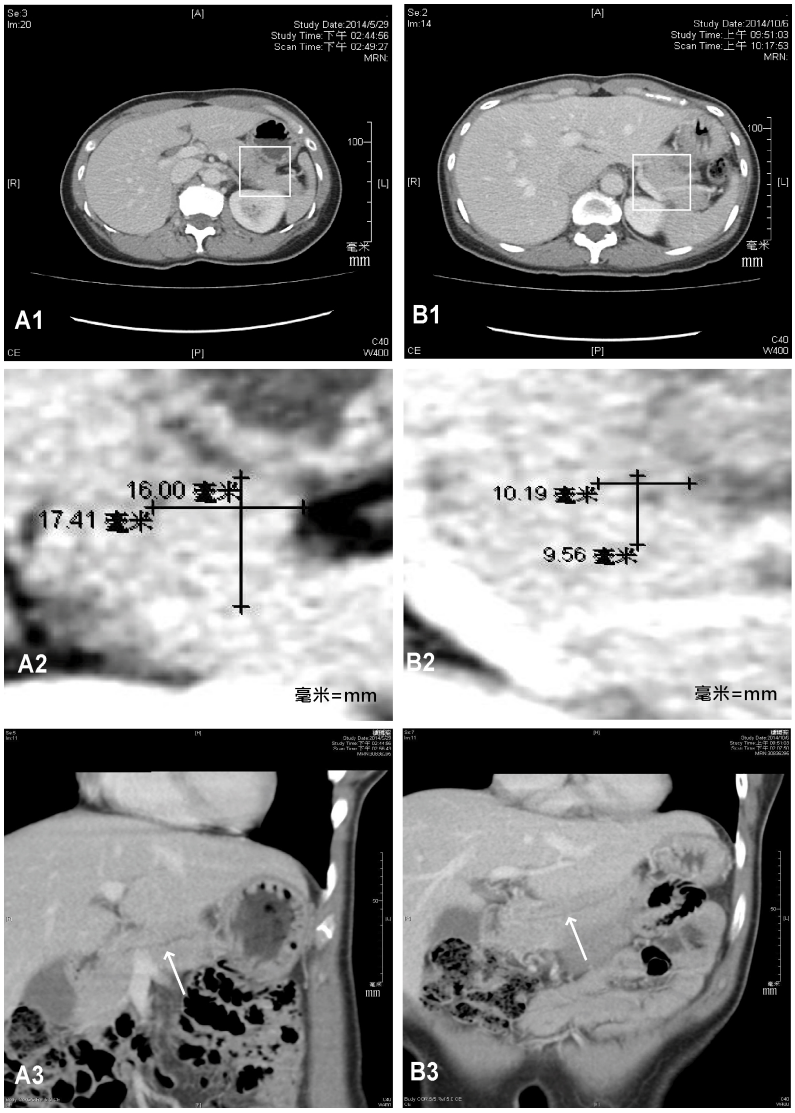

Figure 4. CT scan for suspicious pancreatic cancer IA of case 2. (A) CT scan on May 29, 2014. (A1) An isodense nodule in pancreatic tail (square area). (A2) Magnified photo of the square area of A1, showed the size of the isodense nodule about 1.6 × 1.7 cm. (A3) Dilated tortuous main pancreatic duct of the pancreas with diameter about 0.39 cm (arrow). (B) CT scan on October 6, 2014. (B1) The isodense nodule in pancreatic tail in the same position of the square area of A1. (B2) Magnified photo of the square area of B1 showed the size of the isodense nodule about 1.0 × 1.0 cm. (B3) Main pancreatic duct of pancreas with smooth feature about 0.14 cm in diameter (arrow). CT scan, computed tomography scan.

3.2.2. HR Treatment

The patient refused surgical approach for the possibly poor prognosis of this disease and received HR management from June 5. She performed HR with her hands applied heavily onto the bilateral epigastric area for 5 minutes on each side 2 times a day (**Figure 1(C1)**, **Figure 1(C2)**) and occasionally on bilateral costovertebral angles (**Figure 1(B3)**, **Figure 1(C3)**) and other abdominal areas (**Figure 1(C1)**, **Figure 1(C2)**). CA199 and CA125 which were recorded as 1090.0 and 46.5 before the initiation of HR separately became 170.5 and 50.2 on June 11 and 136.5 and 25.4 on October 3. CT scan on October 6 indicated that the isodense nodule shrank to approximately 1.0 × 1.0 cm in the greatest dimension (rounded from 10.19 × 9.56 mm, **Figure 4(B1)**, **Figure 4(B2)**). Also, the main pancreatic duct became smooth in feature with the diameter decreasing to approximately 0.14 cm (**Figure 4(B3)**). There was no abdominal or back discomfort during this study or history of pancreatitis for this patient.

3.3. Uterine Leiomyosarcoma IB

3.3.1. Disease

This 59-year-old patient suffered from heavy uterine bleeding (7 to 8 fully-soaked pads/day) for 2 months before receiving uterine D & C which was performed on July 31, 2013 and showed atypical muscle tumor. Her uterine bleeding was profuse when she visited our clinic on August 8, 2013.

3.3.2. HR Treatment

Vaginal speculum observations showed that the heavy uterine bleeding immediately decreased to a minimum with a 1-minute HR treatment on each side of the lower abdomen. In a supine position, she then applied HR by press hand over the lower abdomen on each side of the uterus for about 2 - 3 minutes for 3 - 4 times daily (**Figure 1(C1)**). The HR was found to be effective at minimizing heavy uterine bleeding. CT scan on August 15, 2013 showed a heterogeneous lesion about 11.0 × 13.2 cm in uterus. Hysterectomy and bilateral adnexectomy on August 29, 2013 showed 2 myoma-like tumors about 11.5 × 6.6 × 6.5 and 8.1 × 8 × 4.5 cm limited in the uterine body with ill-defined margins. Pathology of both tumors observed with an Olympus light microscope (DP20, Olympus, Tokyo, Japan) showed leiomyosarcoma with no lymph node or other pelvic organ involved (Stage IB, T1N0M0).

3.4. Perineal Brownish Macular Lesion with Chronic Myelogenous Leukemia

3.4.1. Disease

This 39-year-old patient had CML and underwent remission for 1 year via Glivec treatment. Upon admittance to our clinic, we discovered on her left gluteal area, a painless brownish macular lesion about 3.5 × 4.2 cm in dimension and 0.3 cm in thickness which did not respond to antibiotic treatment.

3.4.2. HR Treatment

This patient performed HR for 2 minutes on the perineal lesion (**Figure 1(A3)**) twice daily. With solely HR, the perineal lesion became smaller and resolved 2 weeks later. However, this patient refused a biopsy of the macular lesion.

4. Discussion

Cancer is considered a genetic disease as most cancers have been associated with gene-related changes caused by physical, chemical, infectious, or hereditary factors that impair or activate the gene relating to the occurrence of cancer. Oncogene activation or impaired cancer suppression genes are related to genesis, proliferation or metastasis of cancer cells but researches have shown that most oncogene activation or impaired cancer suppression genes do not cause cancer since the initiated cells usually became apoptotic or killed by host defense systems prior to the promotion to cancer. Studies also show that further proliferation-enhancing signals are required to progress along the pathway towards cancerous growth. Cancer requires multiple steps to manifest. Such steps involve poor immunological response, defective genetic repairing, dysregulated and modified epigenetic presentation, loss of intracellular surveillance for cell death, and alternated intercellular micro-environmental interactions [3]. With understanding these in tumor biology, the medications which target specific biological path-

ways of cancer have been developed and become a corner stone for cancer treatment in this century. However, the plasticity of cancer cells allows for development of selective resistance against target-specific therapeutic agents. Modern treatments for cancer yet remain largely incompetent toward most cancers, especially if cancer metastasis occurs [2].

OuDP appears to be consistently effective for treating a wide variety of diseases in terms of distance between hand and lesion, treatment duration and performance frequency. The effect of OuDP can be significantly increased by decreasing the distance between hand and lesion, increasing treatment duration, and raising treatment frequency. Prompt remission of joint pain, edema of soft tissue by trauma, pain by infection or cessation of uterine bleeding in the studies with OuDP indicate a restoration of normal tissue function [9]. Restoration of normal tissue function may re-establish host defense systems, which will contribute to defense against microorganisms, inflammation, degenerative changes, and tumors [9] [10]. The normalization of function of tumor cells may make them conform to the regulations by apoptosis, growth suppression, and metastatic hindrance that undergo with normal cells. The normalization of tissue function by OuDP apparently not only involves the tumor cell but also the microenvironment in which tumor cells lodge. The tumor microenvironment has been regarded as a main factor for tumor development and metastasis. A normalization of tumor microenvironment will place tumor cells under the circumstances that suppress metastasis, prevent uninhibited proliferation, minimize angiogenesis and eliminate abnormal cells with normalized host immunological systems [6] [12].

A past study of the snapping shrimp has shown that interactions between individual shrimps and other shrimps (with different claw shapes and fiber composition) will induce the change of shape and fiber composition of both claws of the individual shrimp [13]. Our previous study also showed that interactions between patient and HR therapist presented similar results via self-administered HR. There is no significant difference between self- and therapist-performed HR to induce OuDP, but the effect of HR is related to application duration, frequency, and distance. Self-administered HR may increase the efficacy of cancer treatment with increasing the frequency and duration of application by patients themselves. However, this study shows the effect of OuDP for treating oncologic diseases depends on distance between hand and lesion. Thus, the OuDP effect may not be well induced for lesions that cannot be fully accessed.

In 1999, it was noted that cancer patients did not fare better than patients treated decades ago [1]. Since 2000, with recent growing understanding of cancer cell biology, modern medicine has approached various alternative ways as a back-up for conventional cancer treatments. The 5-year relative survival rate for all cancers diagnosed between 2003 and 2009 is 68%, up from 49% in 1975-1977 in USA [2]; however, the morbidity and mortality by cancer is yet much higher than those for most of other diseases. Cancer treatment itself may often impact patients' quality of life due to side effects or complications. An ideal treatment should be effective to ameliorate disease but causes minimal side effects or complications. A recent Swedish statistical study shows there it was discovered that the breast cancer of many patients spontaneously regressed without treatments [14]. It shows spontaneous cancer regression is not rare though the mechanism remains speculative. The OuDP effect shows the capacity to bring about tumor regression, which is comparable with the spontaneous cancer regression reported.

5. Conclusion

In summary, OuDP is induced by the interaction of human bilateral symmetrical features and has proven to accelerate the recovery processes for inflammation, degenerated diseases, tissue dysfunction, and oncological changes. The resolution of non-infectious conditions with OuDP is consistent with the restoration of normal tissue function. This restoration of normal tissue function for cancer indicates to involve not only tumor cells but also the tumor microenvironment, which may make tumor cells conform to the regulations for normal cells as with apoptosis, metastasis suppression, preventing uninhibited proliferation, minimizing angiogenesis and supervision with host immunological systems. However, due to the relatively small sample-size in our study, future studies are warranted to replicate these findings.

Acknowledgements

The authors thank Dr. Yi-Chin Chang (Taipei City Hospital) and Dr. Jan-Show Chu (Taipei Medical University Hospital) for providing pathological photos; thank Dr. Jen-Dar Chen (Taipei City Hospital) and Professor An-Hang Yang (Yang-Ming University) for consultations on radiography and pathology; thank the department of

pathology and laboratory (Taipei City Hospital) for providing the information about staining, immunochemistry and tumor marker analysis; and thank Ms. Yi-Jen Ou for the assistant work.

Conflict of Interest

The authors declare that they have no conflict of interest.

References

[1] Richardson, M.A., Ramirez, T., Russell, N.C. and Moye, L.A. (2014) Coley Toxins Immunotherapy: A Retrospective Review. *Alternative Therapies, Health and Medicine*, **5**, 42-47.

[2] The American Cancer Society (2014) Cancer Facts & Figures 2014. http://www.cancer.org/acs/groups/content/@research/documents/webcontent/acspc-042151.pdf

[3] Hanahan, D. and Weinberg, R.A. (2011) Hallmarks of Cancer: The Next Generation. *Cell*, **144**, 646-674. http://dx.doi.org/10.1016/j.cell.2011.02.013

[4] Musgrove, E.A. and Sutherland, R.L. (2009) Biological Determinants of Endocrine Resistance in Breast Cancer. *Nature Reviews Cancer*, **9**, 631-643. http://dx.doi.org/10.1038/nrc2713

[5] Igney, F.H. and Krammer, P.H. (2002) Immune Escape of Tumors: Apoptosis Resistance and Tumor Counterattack. *Journal of Leukocyte Biology*, **71**, 907-920.

[6] Lorusso, G. and Rüegg, C. (2008) The Tumor Microenvironment and Its Contribution to Tumor Evolution toward Metastasis. *Histochemistry and Cell Biology*, **130**, 1091-1103. http://dx.doi.org/10.1007/s00418-008-0530-8

[7] Ou, M.C., Pang, C.C. and Ou, D. (2011) Abdominal Palpation with Ou MC Manipulation (APOM) for Women with Acute Abdomen Caused by Pelvic Inflammatory Disease: A Pilot Study. *JEM*, **41**, 87-89.

[8] Ou, M.C., Pang, C.C., Ou, D. and Su, C.H. (2012) The Implications of Abdominal Palpation with Ou MC Manipulation for Women with Acute Abdomen. *American Journal of Emergency Medicine*, **30**, 421-425. http://dx.doi.org/10.1016/j.ajem.2011.01.008

[9] Ou, M.C., Ou, D. and Pang, C.C. (2014) A Primitive Approach to Ou MC Decrescendo Phenomenon with a Hands-On Therapy—The Relation between Human Bilateral Symmetry and Disease. *Natural Science*, **2**, 88-98. http://dx.doi.org/10.4236/ns.2014.62013

[10] Ou, M.C., Ou, D. and Pang, C.C. (2014) The Relation between Human Bilateral Symmetry and Disease. *Proceedings of the Physiological Society*, **31**, PCA132. http://www.physoc.org/proceedings/abstract/Proc%20Physiol%20Soc%2031PCA132

[11] Department of Health, Executive Yuan (1993) No.82075656. http://homepage.vghtpe.gov.tw/~ged/listn/listn_a122.htm

[12] Dunn, G.P., Koebel, C.M. and Schreiber, R.D. (2006) Interferons, Immunity and Cancer Immunoediting. *Nature Reviews Immunology*, **6**, 836-848. http://dx.doi.org/10.1038/nri1961

[13] Pearce, J. and Govind, C.K. (1987) Spontaneous Generation of Bilateral Symmetry in the Paired Claws and Closer Muscles of Adult Snapping Shrimps. *Development*, **100**, 57-63.

[14] Zahl, P.H., Gotzsche, P.C. and Mahlen, J. (2011) Natural History of Breast Cancers Detected in the Swedish Mammography Screening Programm: A Cohort Study. *The Lancet Oncology*, **12**, 1118-1124.

Natural Science, 2015, 7, 81-87
Published Online February 2015 in SciRes. http://www.scirp.org/journal/ns
http://dx.doi.org/10.4236/ns.2015.72009

Direct Shoot Regeneration from Callus of *Melicope lunu-ankenda*

Ab. Zuraida Rahman[1], Ayu Nazreena Othman[1], Fatin Liyana Izzati Kamaruddin[1], Aziz Bin Ahmad[2,3]

[1]Biotechnology Research Centre, MARDI Headquarters, Persiaran MARDI-UPM, Serdang, Malaysia
[2]School of Science and Food Technology, Universiti Malaysia Terengganu, Kuala Nerus, Malaysia
[3]Centre for Fundamental and Liberal Education, Universiti Malaysia Terengganu, Kuala Nerus, Malaysia
Email: azuraida@mardi.gov.my, aaziz@umt.edu.my

Received 22 January 2015; accepted 11 February 2015; published 12 February 2015

Abstract

***Melicope lunu-ankenda* is commonly used in traditional medicine. The conventional propagation method for this species is inefficient due to low propagation rate and its lengthy period to maturity. In addition, insufficient planting materials often pose a problem for the plantation sector. The tissue culture technique is best alternative to overcome the problems. The callus induction and direct shoot regeneration protocols for *M. lunu-ankenda* were established. Callus was successfully initiated from leaves explants cultured in MS medium added with 2,4-D at concentrations 0.5 to 5.0 mg/L singly or in combination with NAA at concentrations 1.0 to 10 mg/L. Shoot was regenerated from callus in phytohormone-free medium, BAP at concentrations 0.5 - 5.0 mg/L singly or in combination of BAP with NAA or 2,4-D at concentration 0.5 and 1.0 mg/L, respectively. BAP at 1.0 mg/L induced the highest shoot regeneration rate (80%) and number of plantlet per calli. The established methods might be used for production of phytochemicals and plantlets in large scale.**

Keywords

Melicope lunu-ankenda*, Regeneration, Plant Growth Regulator, *In Vitro

1. Introduction

Melicope lunu-ankenda (Gaertn.), a tree species belonging to the family Rutaceae. It endemic plant to Malaysia and locally known as "Tenggek burung", a popular ulam (salad) consumed raw by Malays. Leaves of this plant are traditionally used to revitalize the body as well as to prevent hypertension. It is also used in Indian traditional medicine to relieve fevers, and as a tonic and for improving complexion. Extracts of the plant were exhibited

How to cite this paper: Rahman, Ab.Z., Othman, A.N., Kamaruddin, F.L.I. and Ahmad, A.B. (2015) Direct Shoot Regeneration from Callus of *Melicope lunu-ankenda*. *Natural Science*, **7**, 81-87. http://dx.doi.org/10.4236/ns.2015.72009

bacteriostatic and fungicidal activity, natural antioxidant and effective anti-inflammatory and immunemodulatory agent [1]. The plant could also serve as leads in the search for anti-quorum sensing compounds [2]. Phytochemical screening shows that the *Melicope* plant containing alkaloid; melicarpine, semecarpine, 8-methoxyplatydesmine [3], dictamnine, confusameline and chromenes [1]. Production of such compounds requires a huge amount of plant materials, at the same time, the resource must be sustained. The conventional propagation method for this uncommon species is inefficient due to low propagation rate and its lengthy period to maturity. In addition, insufficient planting materials is often a problem for the plantation sector. Therefore, there is a need to develop methodologies for mass multiplication of this plant.

Advances in biotechnology have generated new opportunities for *Melicope* genetic improvement and metabolites production. The tissue culture technique is best alternative to overcome the problems. Vegetative propagation through *in vitro* culture techniques of *M. lunu-ankenda* had been previously reported [4]. The genetic improvements of the plant also feasible through somaclonal variation [5]. Such technique is a helpful tool to reduce the time for improvement of woody plant often takes many years using traditional plant-breeding methods [6]. The somaclonal variations techniques were reported to improve citrus against different a biotic stresses, low yield and conserve important citrus genotypes though exploiting somatic cell hybridization [7] and transformation of high yielding cultivars [8] disease free plants. Somaclonal variation exhibited in a wide range of traits including plant height, overall growth habit, flower, fruit and leaf morphology, juvenility, maturity date, disease resistance, yield, virus-free and biochemical characteristics. However, all these highly sophisticated technique requires the presence of highly responsive regeneration protocol. Nonetheless, most reports generally deal with either Solanaceous or cereal crops and limited information has been reported in woody trees.

The present study was to develop an efficient callus initiation system of *M. lunu-ankenda* through tissue culture, which might be used in genetic transformation system and/or efficient and suitable regeneration protocol of the plant in future. Moreover, *in vitro* shoot multiplication would also result in the production of more uniform stocks with high genetic stability. This present study is aimed at developing an efficient mass micropropagation protocol for *M. lunu-ankenda* using shoots as explants. The cell culture would also providing unlimited sources for metabolites production and genetic modification. Furthermore, shoot regeneration from cell culture is the prerequisite for the success in genetic modification. To our knowledge, this is the first report on the shoot regeneration from callus culture on *Melicope*.

2. Material and Methods

2.1. Plant Material and Culture Condition

The *M. lunu-ankenda* plants grown and maintained in a glass house was used as explant. Glass-house conditions were maintained at temperatures 29˚C ± 3˚C with a 12L:12D photoperiod and the relative humidity fluctuated between 50% - 70%. Lateral shoots segments were used to initiate shoot cultures. Explants were cleaned in a detergent (Teepol) solution for 20 min and rinsed in distilled water. Surface sterilization was preceded by immersed in 20% (v/v) Clorox® containing several drops of Tween-20 for 20 min and repeated for another 20 min in 5% (v/v) concentration. Subsequently, rinsed with sterilized distilled water few times. The death tissue were excised and shoot explants were inoculated onto MS medium supplemented with 3% sucrose and 1.0 mg/L BAP. The medium was adjusted to pH 5.8 prior solidified with 0.3% (w/v) gelrite and sterilized by autoclaving at 121˚C and 104 kPa for 15 min. All cultures were incubated in culture room under white light provided with white fluorescent light at intensity of 3000 lux at a photoperiodic 16 h. The room temperature was maintained at 25˚C ± 2˚C. The established *in vitro* plantlets were sub-cultured every three month interval **Figure 1(h)**. These plantlets was used as explant for callus induction.

2.2. Callus Induction

Under aseptic condition, stem of the *in vitro* plantlets were excised in 1 - 2 cm length and inoculated onto callus initiation medium. The medium consisted of MS [9] basal medium, 3% (w/v) sucrose, 3 g/L phytogel and 2,4-D at concentrations of 0, 0.5, 1.0, 3.0 or 5.0 mg/L or NAA at concentrations of 0, 1.0, 3.0, 5.0 or 10 mg/L, or combination of both phytohormones (**Table 1**). All cultures were maintained under light (1200 lux) and monitored weekly. The percentage of explants produced callus and day of callus formed were scored as amount of callus produced at every seven days intervals. Callus induction success was expressed as Percentage of explants induce

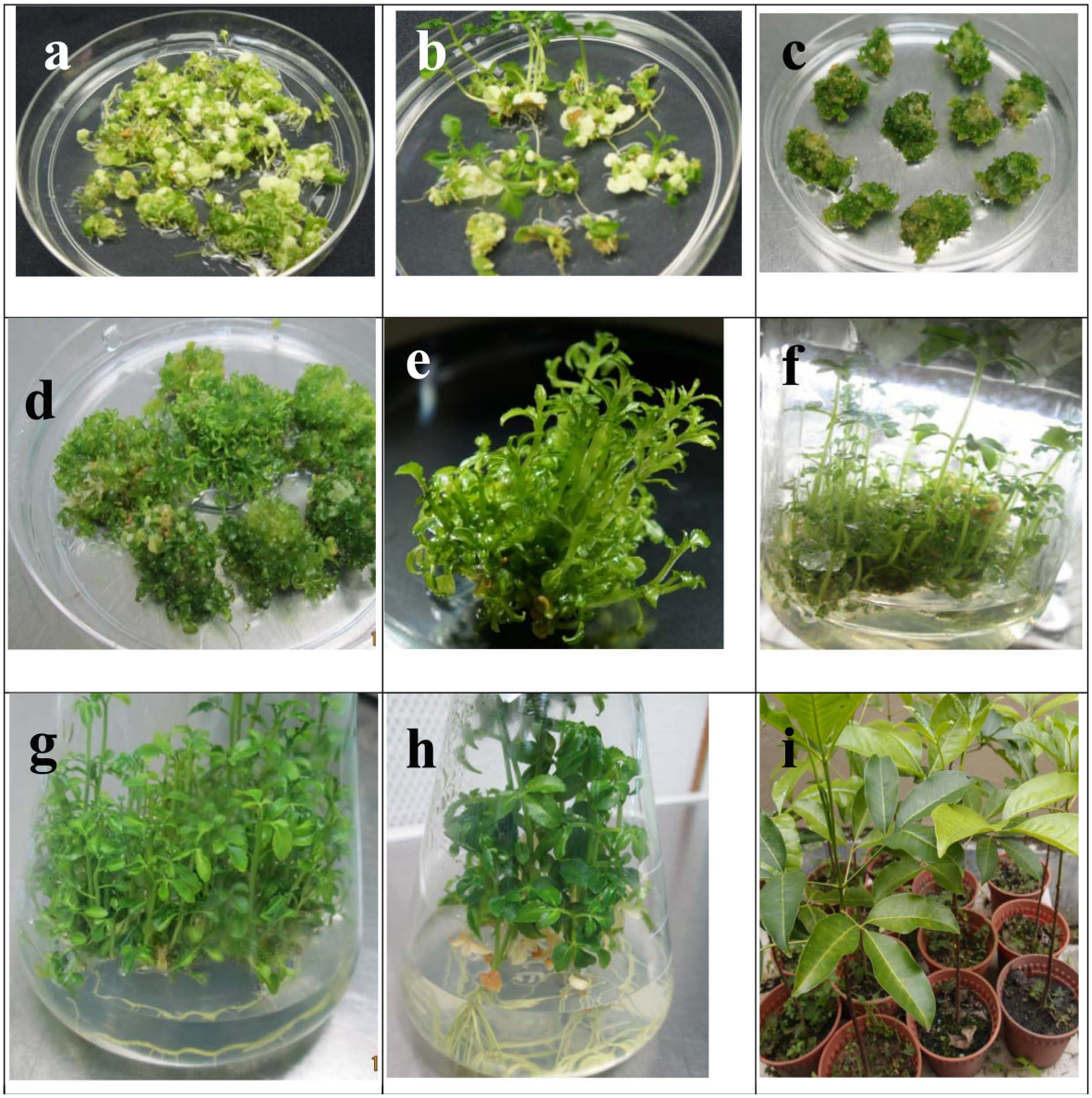

Figure 1. The direct shoots regeneration of *Melicope lunu-ankenda*. Callus were produced from the wounded side of the stems within a month of culture on 2,4-D alone and in combination with NAA (a)-(c); greenish callus were successfully regenerated to plantlets (d)-(g); rooted plantlets (h) *in vitro* plant acclimatization, growth in the net house (i).

callus and weight of green callus after second sub-culture (two months).Any further changes in the coloursof the callus were also recorded.

2.3. Plant Regeneration and Rooting

The yellow-green and dark-green calli were used for induction of shoot and plant regeneration. A small pieces of callus (app.3 gram) were aseptically transferred onto regeneration medium consisted of MS [9] basal medium, 3% (w/v) sucrose, 0.3% (w/v) phytogel and phytohormones; BAP at concentrations of 0, 0.5, 1.0, 3.0 or 5.0 mg/L singly or in combination with NAA at concentrations of 0.5 or 1.0 mg/L, or with 2,4-D at concentrations of 0.5 or 1.0 mg/L, respectively (**Table 2**). All cultures were maintained under a 16 h photoperiod with lighting provided by cool-white fluorescent lamps (100 - 2000 lux). The percentage of calli regenerated to plant and number of plantlets or shoots per clump of green callus were recorded after 45 days of culture. The completely regene-

Table 1. Effect of different combination of 2,4-D and NAA on callus induction of *Melicope lunu-ankenda* on MS medium after 45 days.

Plant growth regulator (mg/L)		Percentage of explants induce callus (%)	Weight of green callus after second sub-culture	Colour of callus
NAA	2,4-D			
0	0	0	-	-
	0.5	25 ± 4.1	0.16 ± 0.01	Yellow-green
	1.0	30 ± 2.2	0.33 ± 0.12	Yellow-green
	3.0	15 ± 3.3	2.11 ± 0.11	Yellow-green
	5.0	10 ± 0.9	0.97 ± 0.23	Yellow-green
1.0	0	0	-	-
	0.5	10 ± 1.1	0.34 ± 0.04	Yellow-green
	1.0	10 ± 1.4	0.56 ± 0.06	Yellow-green
	3.0	54 ± 4.5	4.98 ± 0.87	Yellow-green
	5.0	34 ± 3.1	2.12 ± 0.56	Yellow-green
3.0	0	0	-	-
	0.5	0	0.45 ± 0.05	Yellow-green
	1.0	45 ± 6.7	0.97 ± 0.12	Yellow-green
	3.0	35 ± 2.3	7.81 ± 1.23	Dark-green
	5.0	30 ± 1.1	2.34 ± 0.45	Yellow-green
5.0	0	0	-	-
	0.5	12 ± 2.1	4.56 ± 0.89	Dark-green
	1.0	65 ± 7.2	5.49 ± 1.21	Dark-green
	3.0	50 ± 6.7	6.45 ± 1.24	Dark-green
	5.0	20 ± 2.3	1.89 ± 0.40	Necrotic-green
10.0	0	0	-	-
	0.5	34 ± 3.3	7.50 ± 2.41	Dark-green
	1.0	75 ± 9.5	8.45 ± 0.98	Dark-green
	3.0	55 ± 3.5	6.54 ± 0.89	Necrotic-green

rated plantlets were separated to single plantlet and transferred to MS basal medium containing 0.5 mg/L IBA for root induction. After shoots, the rooted and healthy plantlets were individually transplanted to plastic pots containing hardening medium consisted of top soil:compost mixture (2:1). The plantlets were kept under controlled environment in a net house with 75% shading for 60 days. The survival rate of plantlets was recorded during the period of acclimatization.

2.4. Statistical Analysis

The data (20 replicates per treatment) were subjected to one way analysis of variance (ANOVA) to assess treatment differences and interaction using SPSS version 11.0 software. Significance of differences between means was tested by Duncan's Multiple Range Test ($p < 0.5$).

3. Results and Discussion

3.1. Callus Induction

The effect of different phytohormone on callus induction from stem of *M. lunu-ankenda* were successfully

Table 2. Effect of different combination of NAA, 2,4-D and BAP percentage of regenerating and multiple shoot formation of *Melicope lunu-ankenda* that initiated from green callus.

Plant Growth regulator (mg/L)			Percentage of callus produced shoot (%)	Number of shoot per clump green callus (3 gram)
NAA	2,4-D	BAP		
-	-	0	30 ± 4.5	11 ± 1.1
	-	0.5	70 ± 8.7	27 ± 3.4
	-	1.0	80 ± 9.6	31 ± 6.1
	-	3.0	50 ± 3.4	17 ± 2.3
	-	5.0	35 ± 5.7	12 ± 2.1
0.5	-	0	10 ± 1.3	7 ± 0.9
	-	0.5	35 ± 3.4	18 ± 4.5
	-	1.0	45 ± 6.6	19 ± 1.3
	-	3.0	30 ± 3.2	18 ± 4.5
	-	5.0	15 ± 3.1	6 ± 1.0
1.0	-	0	10 ± 2.1	15 ± 2.2
	-	0.5	35 ± 6.7	18 ± 4.1
	-	1.0	35 ± 8.1	15 ± 2.1
	-	3.0	25 ± 2.3	15 ± 2.4
	-	5.0	0	0
-	0.5	0	0	0
-		0.5	20 ± 2.1	9 ± 0.9
-		1.0	15 ± 2.3	12 ± 2.1
		3.0	0	0
		5.0	5 ± 1.5	8 ± 0.5
-	1.0	0	5 ± 0.9	0
-		0.5	15 ± 0.9	8 ± 0.5
-		1.0	15 ± 1.3	11 ± 1.3
		3.0	10 ± 1.2	0
		5.0	0	0

established (**Table 1**). Yellow to green, friable, non-embryogenic callus were produced from the wounded side of the stems within a month of culture on 2,4-D alone and in combination with NAA (**Figures 1(a)-(c)**). The best response of callus induction (75%) was observed in 1.0 mg/L of 2,4-D + 10 mg/L of NAA with dark-green colour of calli with the highest percentage (30%) in 1.0 mg/L 2,4-D. This was followed with 1.0 mg/L of 2,4-D + 5.0 mg/L of NAA (dark-green callus) and 3.0 mg/L of 2,4-D + 1.0 mg/L of NAA (yellow-greenish), which 65 and 55%, respectively. These results are in conformity with some of the earlier studies on different Rutaceae, which showed good callus induction response under the influence 2,4-D in combination with other phytohormone [10] [11]. Interestingly, 2,4-D combined with NAA at high concentrations (>3 mg/l) was enhanced the size or biomass the green colour of the calli. Green colour normally due to the formation of photosynthetic apparatus, the chlorophyll. A similar phenomena was previously reported in few plant species [11].

3.2. Plant Regeneration

The greenish callus were successfully regenerated to plantlets (**Figures 1(d)-(g)**). The highest percentage of plant regeneration (80%) and the highest number of shoot per calli clump (31 shoots per 3 gram callus) were

obtained in 1.0 mg/L BAP (**Table 2**). In BAP (1.0 mg/L) + NAA or 2,4-D with increasing concentrations (0.5 - 1.0 mg/L), shown a decreases in the plant regeneration as well of number of shoot produced. A similar response was reported [10] on shoot regeneration of citrus callus a member of Rutaceae family. The *in vitro* rooted plantlets transplanted into plastic pots in 75% shading net house were exhibited 98% survival rate after 60 days of transplanting (**Figures 1(h)-(i)**).

4. Conclusion

The callus and plant regeneration protocol were successfully established for *M. lunu-ankenda*. The size, colour and biomass of the calli produced were varies between the induction medium used. Combination of 3.0 mg/L 2,4-D and 1.0 mg/L NAA was the best for callus formation. BAP at concentration 1.0 mg/L was the best for induction of direct shoot regeneration using callus explant. The easily direct shoot regeneration of callus is useful for genetic modification and *in vitro* metabolites production. The protocol developed may aid the sustainable production of the phytochemical and planting material.

Acknowledgements

Authors wish to thank MARDI for providing the research grant and platform for the study.

References

[1] Johnson, A.J., Kumar, R.A., Rasheed, S.A., Chandrika, S.P., Chandrasekhar, A., Baby, S. and Subramoniam, A. (2010) Antipyretic, Analgesic, Anti-Inflammatory and Antioxidant Activities of Two Major Chromenes from *Melicopelunu ankenda*. *Journal of Ethnopharmacology*, **130**, 267-271. http://dx.doi.org/10.1016/j.jep.2010.05.003

[2] Tan, L.Y., Yin, W.F. and Chan, K.G. (2012) Silencing Quorum Sensing through Extracts of *Melicope lunu-ankenda*. *Sensors* (*Basel*), **12**, 4339-4351. http://dx.doi.org/10.3390/s120404339

[3] Chen, J.J., Duh, C.Y., Huang, H.Y. and Chen, I.S. (2003) Furoquinoline Alkaloids and Cytotoxic Constituents from the Leaves of *Melicope semecarpifolia*. *Planta Medica*, **69**, 542-546. http://dx.doi.org/10.1055/s-2003-40637

[4] Zuraida, A.R., Fatin-Liyana, I.K. and Ayu-Nazreena, O. (2014) *In Vitro* Plant Propagation for Rapid Multiplication of *Melicope lunu-ankenda*: A Plant Species of High Medicinal Value. *International Journal of Pharmalogical Bio-Science*, **5**, 1148-1156.

[5] Ravindra, N.S., Ramesh, S.I., Gupta, M.K., Jhang, T., Shukla, A.K., Darokar, M.P. and Kulkarni, R.N. (2012) Evaluation of Somaclonal Variation for Genetic Improvement of Patchouli (*Pogostemon patchouli*), an Exclusively Vegetatively Propagated Aromatic Plant. *Journal of Crop Science and Biotechnology*, **15**, 33-39. http://dx.doi.org/10.1007/s12892-011-0068-5

[6] Nocker, S.V. and Gardiner, S.E. (2014) Breeding Better Cultivars, Faster: Applications of New Technologies for the Rapid Deployment of Superior Horticultural Tree Crops. *Horticulture Research*, **1**, 1-22. http://dx.doi.org/10.1038/hortres.2014.22

[7] Grosser, J.W., Ollitrault, P. and Olivares-Fuster, O. (2000) Somatic Hybridization in Citrus: An Effective Tool to Facilitate Variety Improvement. *In Vitro Cellular & Developmental Biology-Plant*, **36**, 434-449. http://dx.doi.org/10.1007/s11627-000-0080-9

[8] Koltunow, A.M. (2002) Regeneration of West Indian Limes (*Citrus aurantifolia*) Containing Genes for Decreased Seed Set. *Acta Horticulturae*, **535**, 151-157.

[9] Murashige, T. and Skoog, F. (1962) A Revised Medium for Rapid Growth and Bioassays with Tobacco Tissue Cultures. *Physiologia Plantarum*, **15**, 473-497. http://dx.doi.org/10.1111/j.1399-3054.1962.tb08052.x

[10] Savita, Singh, B., Virk, G.S. and Nagpal, A.K. (2011) An Efficient Plant Regeneration Protocol from Callus Cultures of *Citrus jambhiri* Lush. *Physiology Molecular Biology Plants*, **17**, 161-169. http://dx.doi.org/10.1007/s12298-011-0055-9

[11] Singh, N., Meena, M.K. and Patni, V. (2011) Effect of Plant Growth Regulators, Explants Type and Efficient Plantlet Regeneration Protocol through Callus Induction in *Naringicrenulata* (Roxb.) Nicolson and Its Biochemical Investigation. *African Journal of Biotechnology*, **10**, 17769-17777. http://dx.doi.org/10.5897/AJB11.1158

Abbreviations

NAA = 1-naphthaleneacetic acid;
2,4-D = 2,4-dichlorophenoxy acetic acid;
BAP = benzylamino purine;
IBA = indole-3-butyric acid.

Natural Science, 2015, 7, 88-99
Published Online February 2015 in SciRes. http://www.scirp.org/journal/ns
http://dx.doi.org/10.4236/ns.2015.72010

Navier-Stokes Equations—Millennium Prize Problems

Asset A. Durmagambetov, Leyla S. Fazilova

System Research "Factor" Company, Astana, Kazakhstan
Email: asset.durmagambet@gmail.com

Received 6 February 2015; accepted 24 February 2015; published 27 February 2015

Abstract

In this work, we present final solving Millennium Prize Problems formulated by Clay Math. Inst., Cambridge. A new uniform time estimation of the Cauchy problem solution for the Navier-Stokes equations is provided. We also describe the loss of smoothness of classical solutions for the Navier-Stokes equations.

Keywords

Schrödinger's Equation, Potential, Scattering Amplitude, Cauchy Problem, Navier-Stokes Equations, Fourier Transform, The Global Solvability and Uniqueness of the Cauchy Problem, The Loss of Smoothness, The Millennium Prize Problems

1. Introduction

In this work, we present final solving Millennium Prize Problems formulated by Clay Math. Inst., Cambridge in [1]. Before this work, we already had first results in [2]-[4]. The Navier-Stokes existence and smoothness problem concerns the mathematical properties of solutions to the Navier-Stokes equations. These equations describe the motion of a fluid in space. Solutions to the Navier-Stokes equations are used in many practical applications. However, theoretical understanding of the solutions to these equations is incomplete. In particular, solutions of the Navier-Stokes equations often include turbulence, which remains one of the greatest unsolved problems in physics. Even much more basic properties of the solutions to Navier-Stokes have never been proven. For the three-dimensional system of equations, and given some initial conditions, mathematicians have not yet proved that smooth solutions always exist, or that if they do exist, they have bounded energy per unit mass. This is called the Navier-Stokes existence and smoothness problem. Since understanding the Navier-Stokes equations is considered to be the first step to understanding the elusive phenomenon of turbulence, the Clay Mathematics Institute in May 2000 made this problem one of its seven Millennium Prize problems in mathematics. In this paper,

How to cite this paper: Durmagambetov, A.A. and Fazilova, L.S. (2015) Navier-Stokes Equations—Millennium Prize Problems. *Natural Science*, **7**, 88-99. http://dx.doi.org/10.4236/ns.2015.72010

we introduce important explanations results presented in the previous studies in [2]-[4]. We therefore reiterate the basic provisions of the preceding articles to clarify understanding them. First, we consider some ideas for the potential in the inverse scattering problem, and this is then used to estimate of solutions of the Cauchy problem for the Navier-Stokes equations. A similar approach has been developed for one-dimensional nonlinear equations [5]-[8], but to date, there have been no results for the inverse scattering problem for three-dimensional nonlinear equations. This is primarily due to difficulties in solving the three-dimensional inverse scattering problem. This paper is organized as follows: first, we study the inverse scattering problem, resulting in a formula for the scattering potential. Furthermore, with the use of this potential, we obtain uniform time estimates in time of solutions of the Navier-Stokes equations, which suggest the global solvability of the Cauchy problem for the Navier-Stokes equations. Essentially, the present study expands the results for one-dimensional nonlinear equations with inverse scattering methods to multi-dimensional cases. In our opinion, the main achievement is a relatively unchanged projection onto the space of the continuous spectrum for the solution of nonlinear equations that allows focusing only on the behavior associated with the decomposition of the solutions to the discrete spectrum. In the absence of a discrete spectrum, we obtain estimations for the maximum potential in the weaker norms, compared with the norms for Sobolev's spaces.

Consider the operators $H=-\Delta_x+q(x)$ and $H_0=-\Delta_x$ defined in the dense set $W_2^2\left(R^3\right)$ in the space $L_2\left(R^3\right)$; let q be a bounded fast-decreasing function. The operator H is called the Schrödinger's operator. We consider the three-dimensional inverse scattering problem for the Schrödinger operator: the scattering potential must be reconstructed from the scattering amplitude. This problem has been studied by a number of researchers [9] [11] [12] and references therein.

2. Results

Consider Schrödinger's equation:

$$-\Delta_x\Psi+q(x)\Psi=\left|k^2\right|\Psi,\quad k\in C. \tag{1}$$

Let $\Psi_+(k,\theta,x)$ be a solution of (1) with the following asymptotic behavior:

$$\Psi_+(k,\theta,x)=e^{ik\theta x}+\frac{e^{i|k||x|}}{|x|}A(k,\theta',\theta)+o\left(\frac{1}{|x|}\right),\quad |x|\to\infty \tag{2}$$

where $A(k,\theta',\theta)$ is the scattering amplitude and $\theta'=x/|x|$, $\theta\in S^2$ for $k\in\overline{C}^+=\{\mathrm{Im}k\geq 0\}$

$$A(k,\theta',\theta)=\frac{1}{4\pi}\int_{R^3}q(x)\Psi_+(k,\theta,x)e^{-ik\theta' x}\mathrm{d}x. \tag{3}$$

Let us also dene the solution $\Psi_-(k,\theta,x)$ for $k\in\overline{C}^-=\{\mathrm{Im}k<0\}$ as $\Psi_-(k,\theta,x)=\Psi_+(-k,-\theta,x)$
As is well known [9]:

$$\Psi_+(k,\theta,x)-\Psi_-(k,\theta,x)=-\frac{k}{4\pi}\int_{S^2}A(k,\theta',\theta)\Psi_-(k,\theta',x)\mathrm{d}\theta',\quad k\in R. \tag{4}$$

This equation is the key to solving the inverse scattering problem, and was first used by Newton [10] [11] and Somersalo *et al*. [12].

Equation (4) is equivalent to the following:

$$\Psi_+=S\Psi_- \tag{5}$$

where S is a scattering operator with kernel $S(k,l)$, $S(k,l)=\int_{R^3}\Psi_+(k,x)\Psi_-^*(l,x)\mathrm{d}x$.

The following theorem was stated in [9]:

Theorem 1. (The energy and momentum conservation laws) Let $q\in\Re$. Then, $SS^*=I$, $S^*S=I$, where I is a unitary operator.

Definition 1. The set of measurable functions $\Re$ with norm defined by $\|q\|_{\Re}=\int_{R^6}\frac{q(x)q(y)}{|x-y|^2}\mathrm{d}x\mathrm{d}y$ is recognized as being of Rollnik class.

As shown in [13], $\Psi_{\pm}(k,x)$ is an orthonormal system of H eigenfunctions for the continuous spectrum. In addition to the continuous spectrum there are a finite number N of H negative eigenvalues, designated as $-E_j^2$ with corresponding normalized eigenfunctions

$$\psi_j\left(x,-E_j^2\right) \quad \left(j=\overline{1,N}\right)$$

where

$$\psi_j\left(x,-E_j^2\right)\in L_2\left(R^3\right).$$

We present Povzner's results [13] below:

Theorem 2. (Completeness) For both an arbitrary $f\in L_2\left(R^3\right)$ and for H eigenfunctions, Parseval's identity is valid.

$$\left|f\right|_{L_2}^2=\left(P_D f,P_D f\right)+\left(P_{A_C} f,P_{A_C} f\right)$$

$$P_D f=\sum_{j=1}^{N} f_j\psi_j\left(x,-E_j\right),\quad P_{A_C} f=\int_0^{\infty}\int_{S^2} s^2\overline{f}(s)\Psi_{+}(s,\theta,x)\mathrm{d}\theta\mathrm{d}s \tag{6}$$

where $\overline{f}$ and f_j are Fourier coefficients for the continuous and discrete cases.

Theorem 3. (Birman-Schwinger estimation). Let $q\in\Re$. Then, the number of discrete eigenvalues can be estimated as:

$$N(q)\le\frac{1}{(4\pi)^2}\int_{R^3}\int_{R^3}\frac{q(x)q(y)}{|x-y|^2}\mathrm{d}x\mathrm{d}y. \tag{7}$$

This theorem was proved in [14].

Let us introduce the following notation:

$$NA=\int_{S^2}A(k,\theta',\theta)\mathrm{d}\theta \quad \text{for} \quad f(k,\theta',x),\quad Df=\int_{S^2}A(k,\theta',\theta)\,f(k,\theta',x)\mathrm{d}\theta' \tag{8}$$

$$\phi_0\left(\sqrt{z},\theta,x\right)=e^{i\sqrt{z}\theta x},\quad \Phi\left(\sqrt{z},\theta',x\right)=\left(\Psi_{+}\left(\sqrt{z},\theta',x\right)-e^{i\sqrt{z}\theta x}\right)\Delta \tag{9}$$

where

$$\Delta=\prod_{j=1}^{N}\left[\left(k+iE_j\right)/\left(k-iE_j\right)\right].$$

We define the operators $T_{\pm}$, T for $f\in W_2^1(R)$ as follows:

$$T_{+}f=\frac{1}{2\pi i}\lim_{\mathrm{Im}z\to 0}\int_{-\infty}^{\infty}\frac{f(s)}{s-z}\mathrm{d}s,\ \ \mathrm{Im}z>0;\quad T_{-}f=\frac{1}{2\pi i}\lim_{\mathrm{Im}z\to 0}\int_{-\infty}^{\infty}\frac{f(s)}{s-z}\mathrm{d}s,\ \ \mathrm{Im}z<0 \tag{10}$$

$$Tf=\frac{1}{2}\left(T_{+}+T_{-}\right)f. \tag{11}$$

Consider the Riemann problem of finding a function Φ, that is analytic in the complex plane with a cut along the real axis. Values of Φ on the upper and lower sides of the cut are denoted Φ_{+} and Φ_{-} respectively. The following presents the results of [15]:

Lemma 1.

$$TT=\frac{1}{4}I,\ \ TT_{+}=\frac{1}{2}T_{+},\ \ TT_{-}=-\frac{1}{2}T_{-},\ \ T_{+}=T+\frac{1}{2}I,\ \ T_{-}=T-\frac{1}{2}I \tag{12}$$

Theorem 4. Let $q\in\Re$, $g=\Phi_{+}-\Phi_{-}$; then

$$\Phi_{\pm}=T_{\pm}g. \tag{13}$$

The proof of the above follows from the classic results for the Riemann problem.

Lemma 2. Let $q\in\Re,\ g_{+}=g\left(\sqrt{z},\theta,x\right),\ g_{-}=g\left(\sqrt{z},-\theta,x\right)$

Then,

$$\Psi_+\left(\sqrt{z},\theta,x\right)\Delta=\left(T_+g_++e^{i\sqrt{z}\theta x}\right),\quad \Psi_-\left(\sqrt{z},\theta,x\right)\Delta=\left(T_-g_-+e^{-i\sqrt{z}\theta x}\right). \tag{14}$$

The proof of the above follows from the definitions of g, Φ_+, Φ_- and Ψ_+, Ψ_-.

Lemma 3. Let $q\in\Re$, $A_+=A\left(\sqrt{z},\theta,x\right)$, $A_-=A\left(\sqrt{z},-\theta,x\right)$

Then,

$$A\left(k,\theta',\theta\right)\Delta=T_+\left(A_+\Delta-A_-\Delta\right). \tag{15}$$

The proof of the above again follows from the definitions of the functions g, Φ_+, Φ_- and Ψ_+, Ψ_-.

Lemma 4. Let $q\in\Re$. Then,

$$NA_+\Delta=NT_+(DA_-\Delta). \tag{16}$$

The proof of the above follows from the definitions of g, Φ_+, Φ_- and Ψ_+, Ψ_- and Theorem 1.

Lemma 5. Let $q\in\Re$. Then,

$$\left|NT\left(A_+\right)\right|\le 2\left|NA_+\right|. \tag{17}$$

The proof of the above follows from the definitions of g, Φ_+, Φ_- and Ψ_+, Ψ_- and Lemma 4 and dispersions relations for analytics functions.

Definition 2. Denote by TA the set of functions $f\left(k,\theta,\theta'\right)$ with the norm

$$\left\|f\right\|_{\mathrm{TA}}=\sup_{\theta,k,\theta'}\left(\left|Tf\right|+\left|f\right|\right)<\infty.$$

Definition 3. Denote by $\Re_{(I-T_-D)}$ the set of functions g such that $g=\left(I-T_-D\right)f$, for any $f\in\mathrm{TA}$.

Lemma 6. Suppose $\left\|A\right\|_{\mathrm{TA}}<\alpha<1$. Then, the operator $\left(I-T_-D\right)$, defined on the setTA has an inverse defined on $\Re_{(I-T_-D)}$.

The proof of the above follows from the definitions of D, T_- and the conditions of Lemma 6.

Lemma 7. Let $q\in\Re$, and assume that $\left(I-T_\pm D\right)^{-1}$ exists. Then,

$$g=T_+g-T_-g,\quad T_-g_-=\left(I-T_-D\right)^{-1}T_-D\phi_0,\quad \Psi_-=\frac{1}{\Delta}\left(I-T_-D\right)^{-1}T_-D\phi_0+\phi_0. \tag{18}$$

The proof of the above follows from the denitions of g, Φ_+, Φ_- and Ψ_+, Ψ_- and Equation (4).

Lemma 8. Let $q\in\Re$, and assume that $\left(I-T_\pm D\right)^{-1}$ exists. Then,

$$\Psi_-=\sum_{i=1}^{\infty}\left(-\frac{1}{\Delta}T_-D\right)^i\phi_0+\phi_0,\quad \frac{1}{\Delta}T_-D+\overline{\frac{1}{\Delta}T_-D}=\frac{1}{\Delta}T_-D\overline{\frac{1}{\Delta}T_-D}+\overline{\frac{1}{\Delta}T_-D}\frac{1}{\Delta}T_-D+Q_3 \tag{19}$$

where Q_3 represents terms of highest order of T_-D.

The proof. Using

$$\int_{R^3}\Psi_-\left(x,k\right)*\overline{\Psi_-\left(x,l\right)}\mathrm{d}x=\delta\left(k-l\right),\quad \int_{R^3}\phi_0\left(x,k\right)*\overline{\phi_0\left(x,l\right)}\mathrm{d}x=\delta\left(k-l\right)$$

and (18) we get proof.

Lemma 9. Let $q\in\Re$. Then,

$$q=\lim_{z\to\infty}\left[H_0\Psi_-/\Psi_-\right]. \tag{20}$$

The lemma can be proved by substituting Ψ_+, Ψ_- into Equation (1).

Lemma 10. Let $q\in\Re$, and assume that $\left(I-T_-D\right)^{-1}$ exists. Then,

$$q=\lim_{z\to\infty}\left[\left(\frac{1}{\Delta}N\left(I-T_-D\right)^{-1}T_-DH_0\phi_0\right)\Big/\left(\frac{1}{\Delta}N\left(I-T_-D\right)^{-1}T_-DH_0\phi_0+N\phi_0\right)\right]. \tag{21}$$

The proof of the above follows from the definitions of N, Ψ_+, Ψ_- and Lemma 7.

Lemma 11. Let $q\in\Re$. Then $\left\|D\right\|\le 2$.

The proof of the above follows from the definition of *D* and the unitary nature of *S*.

Lemma 12. Let $q \in \Re \cap L_4\left(R^3\right)$. Then,

$$E_j^2 \le \int_{R^3} |q(x)| |\psi_j|^2 \, dx \tag{22}$$

$$\max_x |\psi_j(x)| \le 2 \|q\psi_j\|_{L_2\left(R^3\right)}. \tag{23}$$

The proof of the above follows from the definitions of E_j^2, ψ_j, and (1).

Lemma 13. Let $q \in \Re \cap L_2\left(R^3\right)$, and $\|A\|_{\mathrm{TA}} < \alpha < 1$. Then,

$$\left[\Psi_{\pm}|q|\right]_{x=0} \le \sum_{i=1}^{\infty} \left(C_0 \|NA\|_{|k|=0}\right)^i. \tag{24}$$

To prove this result, one should calculate Ψ_+, Ψ_- using (18).

$$\Psi_{\pm} q = \Delta \Psi_{\pm} \tag{25}$$

Using the notation that:

$$\tilde{q}(k) = \int_{R^3} q(x) e^{i(k,x)} dx, \quad \tilde{q}(k-l) = \int_{R^3} q(x) e^{i(k-l,x)} dx, \quad Qq = \int_{R^3} q(x) e^{i(k-l,x)} dx$$

$$Q_E q = \int_{R^3} q(x) e^{i(k-l,x)} dx\Big|_{|k|=|l|}, \quad NQq = \int_{S^2} Qq(k,\theta',\theta) d\theta.$$

For $f = f(k,\theta',x)$

$$Df = k \int_{S^2} A(k,\theta',\theta) f(k,\theta',x) d\theta'. \tag{26}$$

Lemma 14. Let $q \in \Re \cap L_2\left(R^3\right)$, and $\|\mathrm{TA}\|_{\mathrm{TA}} < \alpha < 1$. Then,

$$\|TNA\|_{L_2} < C \|TQq\|_{L_2}, \quad \|NA\|_{L_2} < C \|Qq\|_{L_2}. \tag{27}$$

To prove this result, one should Ψ_+, Ψ_- using Lemma 7.

$$q = \Delta \Psi_{\pm} / \Psi_{\pm}. \tag{28}$$

Using Lemma 7.

Lemma 15. Let $q \in \Re \cap L_2\left(R^3\right)$, and $\|A\|_{\mathrm{TA}} < \alpha < 1$. Then,

$$\Psi_{\pm} \|q\|_{x=0} \le \sum_{i=1}^{\infty} \left(C_0 \|TNA\|_{|k|=0}\right)^i \tag{29}$$

$$\Psi_{\pm} \|q\|_{x=0} \le \sum_{i=1}^{\infty} \left(C_0 \|TQq\|_{|k|=0}\right)^i. \tag{30}$$

To prove this result, one should calculate A using Lemma 7.

Lemma 16. Let $q \in \Re$ and

$$\max_k |\tilde{q}| < \infty.$$

Then,

$$\int_{R^3} \int_{R^3} \frac{q(x) q(y)}{|x-y|^2} dx dy \le C \left(|q|_{L_2} + \max_k |\tilde{q}|\right)^2. \tag{31}$$

A proof of this lemma can be obtained using Plancherel's theorem.

Lemma 17. Let $q \in \Re \cap L_2\left(R^3\right)$ and

$$\|q\|_{L_2} + \max_k |\tilde{q}| < \alpha < 1.$$

Then,

$$\Psi_{\pm}|_{x=0} > 1 - \alpha/(1-\alpha) \tag{32}$$

$$\left\|q\right\|_{x=0} \le \sum_{i=1}^{\infty}\left(C_0 \left\|TQq\right\|_{|k|=0}\right)^i. \tag{33}$$

To prove this result, one should calculate $\Psi_{\pm}\big|_{x=0}$.

3. Cauchy Problem for the Navier-Stokes Equation

Numerous studies of the Navier-Stokes equations have been devoted to the problem of the smoothness of its solutions. A good overview of these studies is given in [16]-[20]. The spatial differentiability of the solutions is an important factor, this controls their evolution. Obviously, differentiable solutions do not provide an effective description of turbulence. Nevertheless, the global solvability and differentiability of the solutions has not been proven, and therefore the problem of describing turbulence remains open. It is interesting to study the properties of the Fourier transform of solutions of the Navier-Stokes equations. Of particular interest is how they can be used in the description of turbulence, and whether they are differentiable. The differentiability of such Fourier transforms appears to be related to the appearance or disappearance of resonance, as this implies the absence of large energy flows from small to large harmonics, which in turn precludes the appearance of turbulence. Thus, obtaining uniform global estimations of the Fourier transform of solutions of the Navier-Stokes equations means that the principle modeling of complex flows and related calculations will be based on the Fourier transform method. The authors are continuing to research these issues in relation to a numerical weather prediction model; this paper provides a theoretical justification for this approach. Consider the Cauchy problem for the Navier-Stokes equations:

$$q_t - v\Delta q + \left(q, \nabla q\right) = -\nabla p + f\left(x,t\right), \quad \operatorname{div} q = 0 \tag{34}$$

$$q\big|_{t=0} = q_0\left(x\right) \tag{35}$$

in the domain $Q_T = R^3 \times \left(0,T\right)$, where:

$$\operatorname{div} q_0 = 0. \tag{36}$$

The problem defined by (34), (35), (36) has at least one weak solution $\left(q, p\right)$ in the so-called Leray-Hopf class [16].

The following results have been proved [17]:

Theorem 5. If

$$q_0 \in W_2^1\left(R^3\right), \quad f \in L_2\left(Q_T\right) \tag{37}$$

there is a single generalized solution of (34), (35), (36) in the domain Q_{T_1}, $T_1 \in \left[0,T\right]$, satisfying the following conditions:

$$q_t,\ \nabla^2 q,\ \nabla p \in L\left(Q_T\right). \tag{38}$$

Note that T_1 depends on q_0 and f.

Lemma 18. Let $q_0 \in W_2^1\left(R^3\right)$, $f \in L_2\left(Q_T\right)$. Then,

$$\sup_{0\le t\le T}\left\|q\right\|_{L_2\left(R^3\right)}^2 + \int_0^t \left\|\nabla q\right\|_{L_2\left(R^3\right)}^2 \mathrm{d}\tau \le \left\|q_0\right\|_{L_2\left(R^3\right)}^2 + \left\|f\right\|_{L_2\left(Q_T\right)}. \tag{39}$$

Our goal is to provide global estimations for the Fourier transforms of the derivatives of the solutions to the Navier-Stokes Equations (34)-(36) without requiring the initial velocity and force to be small. We obtain the following uniform time estimation.

Statement 1. The solution of (34), (35), (36) according to Theorem 5 satisfies:

$$\tilde{q} = \tilde{q}_0 + \int_{R^3} e^{-v|k|^2(t-\tau)}\left(\left[\left(q\tilde{\nabla}\right)q\right] + \tilde{F}\right)\mathrm{d}\tau \tag{40}$$

where $F = -\nabla p + f$.

This follows from the definition of the Fourier transform and the theory of linear differential equations.

Statement 2. The solution of (34), (35), (36) satisfies:

$$\tilde{p} = \sum_{i,j} \frac{k_i k_j}{|k|^2} \tilde{q}_i \tilde{q}_j + i \sum_i \frac{k_i}{|k|^2} \tilde{f}_i \tag{41}$$

and the following estimations:

$$\|p\|_{L_2(R^3)} \le 3 \|\nabla q\|^{3/2}_{L_2(R^3)} \|q\|^{1/2}_{L_2(R^3)} \tag{42}$$

$$|\nabla \tilde{p}|_{L_2(R^3)} \le \frac{|\tilde{q}^2|}{|k|} + \frac{|\tilde{f}|}{|k|^2} + \frac{1}{|k|} |\nabla \tilde{f}| + 3 |\nabla \tilde{q}^2|. \tag{43}$$

This expression for p is obtained using div and the Fourier transform presentation.

Lemma 19. The solution of (34), (35), (36) in Theorem 5 satisfies the following inequalities:

$$\sup_{0 \le t \le T} \|NQq\|^2_{L_2(R^3)} + \int_0^t \|k^2 NQq\|^2_{L_2(R^3)} \, d\tau \le \|NQq_0\|^2_{L_2(R^3)} + \|Qf\|_{L_2(Q_T)}. \tag{44}$$

Proof this follows from the a priory estimation of Lemma18 and conditions of Lemma 19.

Lemma 20. Let $Qq_0 \in W_2^1(R^3)$, $f \in L_2(Q_T)$ Then, the solution of (34), (35), (36) in Theorem 5 satisfies 2 the following inequalities:

$$\sup_{\theta, \sup_{0 \le t \le T}} \left[\|Qq\|^2_{L_2(R^3)} + \int_0^t \|k^2 Qq\|^2_{L_2(R^3)} \, d\tau \right] \le \sup_{\theta} \left[\|Qq_0\|^2_{L_2(R^3)} + \|f\|_{L_2(Q_T)} \right]. \tag{45}$$

Proof this follows from the a priory estimation of Lemma18 and conditions of Lemma 20.

Lemma 21. The solution of (34), (35), (36) in Theorem 5 satisfies the following inequalities:

$$\int_{R^3} |x|^2 |q|^2 \, dx + \int_0^t \int_{R^3} |x|^2 |\nabla q|^2 \, dx d\tau \le \text{const}, \quad \int_{R^3} |x|^4 |q|^2 \, dx + \int_0^t \int_{R^3} |x|^4 |\nabla q|^2 \, dx d\tau \le \text{const} \tag{46}$$

or

$$\|\nabla \tilde{q}\|_{L_2(R^3)} + \int_0^t \int_{R^3} |k|^2 |\tilde{\nabla} q|^2 \, dk d\tau \le \text{const}, \quad \|\nabla^2 \tilde{q}\|_{L_2(R^3)} + \int_0^t \int_{R^3} |k|^2 |\tilde{\nabla}^2 q|^2 \, dk d\tau \le \text{const}. \tag{47}$$

Proof this follows from the a priory estimation of Lemma18, conditions of Lemma 19, the Navier-Stokes equations.

Lemma 22. The solution of (34), (35), (36) satisfies the following inequalities:

$$\max_k |\tilde{q}| \le \max_k |\tilde{q}_0| + \frac{T}{2} \sup_{0 \le t \le T} \|q\|^2_{L_2(R^3)} + \int_0^t \|\nabla q\|^2_{L_2(R^3)} \, d\tau \tag{48}$$

$$\max_k |\nabla \tilde{q}| \le \max_k |\nabla \tilde{q}_0| + \frac{T}{2} \sup_{0 \le t \le T} \|\nabla \tilde{q}\|_{L_2(R^3)} + \int_0^t \int_{R^3} |k|^2 \|\nabla \tilde{q}\|^2_{L_2(R^3)} \, dk d\tau \tag{49}$$

$$\max_k |\nabla^2 \tilde{q}| \le \max_k |\nabla^2 \tilde{q}_0| + \frac{T}{2} \sup_{0 \le t \le T} \|\nabla^2 \tilde{q}\|_{L_2(R^3)} + \int_0^t \int_{R^3} |k|^2 \|\nabla^2 \tilde{q}\|^2_{L_2(R^3)} \, dk d\tau. \tag{50}$$

Proof this follows from the a priory estimation of Lemma 18, conditions of Lemma 22, the Navier-Stokes equations.

Lemma 23. The solution of (34), (35), (36) according to Theorem 5 satisfies $C_i \le \text{const}$, $\left(i = \overline{0,2,4}\right)$, where:

$$C_0 = \int_0^t |\tilde{F}_1|^2 \, d\tau, \quad F_1 = (q, \nabla) q + F, \quad C_2 = \int_0^t |\nabla \tilde{F}_1|^2 \, d\tau, \quad C_4 = \int_0^t |\nabla^2 \tilde{F}_1|^2 \, d\tau. \tag{51}$$

Proof this follows from the a priory estimation of Lemma18, the Navier-Stokes equations.

Lemma 24.Weak solution of problem (34), (35), (36) from Theorem 5 satisfies the following inequalities:

$$|NQq| \le zM_1, \quad \left| \frac{\partial NQq}{\partial z} \right| \le zM_2, \quad \left| \frac{\partial^2 NQq}{\partial z^2} \right| \le zM_3$$

where M_1, M_2, M_3 are limited.

Let is prove the first estimate. These inequalities

$$\left|Qq(z,t)\right| \le \frac{z}{2}\int_0^{\pi}\int_0^{2\pi}\left|\tilde{q}\left(z\left(e_k - e_p\right),t\right)\right|\mathrm{d}e_p \le 2\pi z \max_k\left|\tilde{q}\right| \le zM_1$$

where $M_1 = \text{const}$.

Proof now this follows from the a priori estimation of Lemma 18, conditions of Lemma 24, the Navier-Stokes equations.

The rest of estimates are proved similarly.

Lemma 25. Suppose that $q \in \Re$ and $\max_k\left|\tilde{q}\right| < \infty$

Then,

$$\int_{R^3}\int_{R^3}\frac{q(c)q(y)}{\left|x-y\right|^2}\mathrm{d}x\mathrm{d}y \le C\left(\left|q\right|_{L_2} + \max_k\left|\tilde{q}\right|\right)^2.$$

Proof. Using Plansherel's theorem, we get the statement of the lemma.

This proves Lemma 25.

Lemma 26. Weak solution of problem (34), (35), (36) from Theorem 5 satisfies the following inequalities

$$\left|Qq\right| \le \left|Qq_0\right| + \left(\frac{1}{2\nu}\right)^{\frac{1}{2}}\frac{C_0^{\frac{1}{2}}}{z\left|e_k - e_\lambda\right|} \tag{52}$$

where

$$C_0 = \int_0^t\left|\tilde{F}_1\right|^2\mathrm{d}\tau, \quad F_1 = (q,\nabla)q + F.$$

Proof. From (40) we get

$$\left|Qq\right| \le \left|Qq_0\right| + \left|\int_0^t e^{-\nu z^2\left|e_k - e_\lambda\right|^2(t-\tau)}\tilde{F}_1\left(z\left(e_k - e_\lambda\right),\tau\right)\mathrm{d}\tau\right| \tag{53}$$

where

$$F_1 = (q,\nabla)q + F.$$

Using the notation

$$I = \left|\int_0^t e^{-\nu z^2\left|e_k - e_\lambda\right|^2(t-\tau)}\tilde{F}_1\left(z\left(e_k - e_\lambda\right),\tau\right)\mathrm{d}\tau\right|$$

taking into account Holder's inequality in I we obtain:

$$I \le \left(\int_0^t\left|e^{-\nu z^2\left|e_k - e_\lambda\right|^2(t-\tau)}\right|^p\mathrm{d}\tau\right)^{\frac{1}{p}}\left(\int_0^t\left|\tilde{F}_1\right|^q\mathrm{d}\tau\right)^{\frac{1}{q}} \tag{53}$$

where p and q satisfies the equality $1/p + 1/q = 1$. Suppose $p = q = 2$. Then

$$I \le \left(\frac{1}{2\nu}\right)^{\frac{1}{2}}\frac{\left(\int_0^t\left|\tilde{F}_1\right|^2\mathrm{d}\tau\right)^{\frac{1}{2}}}{z\left|e_k - e_\lambda\right|}.$$

Taking into consideration the estimate I in (53), we obtain the statement of the lemma.

This proves Lemma 26.

Lemma 27. Weak solution of problem (34), (35), (36) from Theorem 5 satisfies the following inequalities

$$\left|\frac{\partial Qq}{\partial z}\right| \le \left|\frac{\partial Qq_0}{\partial z}\right| + 4\alpha\left(\frac{1}{\nu}\right)^{\frac{1}{2}}\frac{C_0^{\frac{1}{2}}}{z^2\left|e_k - e_\lambda\right|} + \left(\frac{1}{2\nu}\right)^{\frac{1}{2}}\frac{C_2^{\frac{1}{2}}}{z\left|e_k - e_\lambda\right|}, \text{ where } C_2 = \int_0^t\left|\frac{\partial\tilde{F}_1}{\partial z}\right|^2\mathrm{d}\tau. \tag{54}$$

Proof. The underwritten inequalities follows from representation (40)

$$\left|\frac{\partial Qq}{\partial z}\right| \le \left|\frac{\partial Qq_0}{\partial z}\right| + 2\nu z\left|e_k - e_\lambda\right|^2 \left|\int_0^t (t-\tau) e^{-\nu z^2 |e_k - e_\lambda|^2 (t-\tau)} \tilde{F}_1\left(z(e_k - e_\lambda), \tau\right) \mathrm{d}\tau\right|$$
$$+ \left|\int_0^t e^{-\nu z^2 |e_k - e_\lambda|^2 (t-\tau)} \frac{\partial \tilde{F}_1}{\partial z}\left(z(e_k - e_\lambda), \tau\right) \mathrm{d}\tau\right|,$$

Let us introduce the following denotation

$$I_1 = 2\nu z\left|e_k - e_\lambda\right|^2 \left|\int_0^t (t-\tau) e^{-\nu z^2 |e_k - e_\lambda|^2 (t-\tau)} \tilde{F}_1\left(z(e_k - e_\lambda), \tau\right) \mathrm{d}\tau\right|$$

$$I_2 = \left|\int_0^t e^{-\nu z^2 |e_k - e_\lambda|^2 (t-\tau)} \frac{\partial \tilde{F}_1}{\partial z}\left(z(e_k - e_\lambda), \tau\right) \mathrm{d}\tau\right|$$

then

$$\left|\frac{\partial Qq}{\partial z}\right| \le \left|\frac{\partial Qq_0}{\partial z}\right| + I_1 + I_2.$$

Estimate I_1 by means of

$$\sup_t \left|t^m e^{-t}\right| < \alpha$$

where $m > 0$ we obtain

$$I_1 \le \frac{4\alpha}{z}\left|\int_0^t e^{-\nu z^2 |e_k - e_\lambda|^2 \frac{t-\tau}{2}} \tilde{F}_1\left(z(e_k - e_\lambda), \tau\right) \mathrm{d}\tau\right|.$$

On applying Holder's inequality, we get

$$I_1 \le \frac{4\alpha}{z}\left(\int_0^t \left|e^{-\nu z^2 |e_k - e_\lambda|^2 \frac{t-\tau}{2}}\right|^p \mathrm{d}\tau\right)^{\frac{1}{p}} \left(\int_0^t \left|\tilde{F}_1\right|^q \mathrm{d}\tau\right)^{\frac{1}{q}}$$

where p, q satisfies the equality $1/p + 1/q = 1$.

For $p = q = 2$ we have

$$I_1 \le 4\alpha\left(\frac{1}{\nu}\right)^{\frac{1}{2}} \frac{C_0^{\frac{1}{2}}}{z^2\left|e_k - e_\lambda\right|}, \quad I_2 \le \left(\frac{1}{2\nu}\right)^{\frac{1}{2}} \frac{C_2^{\frac{1}{2}}}{z\left|e_k - e_\lambda\right|}, \quad C_2 = \int_0^t \left|\frac{\partial \tilde{F}_1}{\partial z}\right|^2 \mathrm{d}\tau.$$

Inserting I_1, I_2 in to

$$\left|\frac{\partial \tilde{q}}{\partial z}\right|$$

we obtain the statement of the lemma.

This completes the proof of Lemma 27.

Lemma 28. Weak solution of problem (34), (35), (36) from Theorem 5 satisfies the following inequalities

$$\begin{aligned} &|NQq| \le C, \quad |TNQq| \le C, \quad |Qq| \le C, \quad |TQq| \le C, \quad |NQ_E q| \le C, \\ &|TNQ_E q| \le C, \quad |Q_E q| \le C, \quad |TQ_E q| \le C \end{aligned} \tag{55}$$

where $C = \text{const}$

Lemma 25. Let $q \in \Re$ and

$$\max_k |\tilde{q}| < \infty.$$

Then,

$$N(q) \le \int_{R^3}\int_{R^3} \frac{q(x)q(y)}{|x-y|^2}\mathrm{d}x\mathrm{d}y \le C\left(|q|_{L_2} + \max_k |\tilde{q}|\right)^2. \tag{56}$$

A proof of this lemma can be obtained using Plancherel's theorem.

We now obtain uniform time estimations for Rollnik's norms of the solutions of (34), (35), (36).The following (and main) goal is to obtain the same estimations for $\max_k |q|$—velocity components of the Cauchy problem for the Navier-Stokes equations.

Let's consider the influence of the following large scale transformations in Navier-Stokes' equation on

$$K = \frac{\nu^{\frac{1}{2}}}{\nu^{\frac{1}{2}} - 4\pi C C_0^{\frac{1}{2}}}, \quad t' = tA, \quad \nu' = \frac{\nu}{A}, \quad F_0' = \frac{F_0}{A^2}.$$

Statement 3. Let

$$A = \frac{4}{\nu^{\frac{1}{3}}\left(CC_0+1\right)^{\frac{2}{3}}}, \quad \text{then} \quad K \le \frac{8}{7}.$$

Proof. By the definitions C and C_0 we have

$$K = \left(\frac{\nu}{A}\right)^{\frac{1}{2}}\left(\left(\frac{\nu}{A}\right)^{\frac{1}{2}} - \frac{4\pi CC_0}{A^2}\right)^{-1} = \nu^{\frac{1}{2}}\left(\nu^{\frac{1}{2}} - \frac{4\pi CC_0}{A^{3/2}}\right)^{-1} < \frac{8}{7}.$$

This proves Statement 3.

Theorem 6. Let

$$q_0 \in W_2^2\left(R^3\right), \quad \nabla^2\tilde{q}_0 \in L_2\left(R^3\right), \quad f \in L_2\left(Q_T\right), \quad \tilde{f} \in L_1\left(Q_T\right)\cap L_2\left(R^3\right), \quad \nabla^2\tilde{f} \in L_1\left(Q_T\right)\cap L_2\left(R^3\right)$$

and

$$\max_k \|Qq_0\|_{L_2} \le \text{const}, \quad \max_k \|Qf\|_{L_2} \le \text{const}, \quad \max_k \|Q_E q_0\|_{L_2} \le \text{const}, \quad \max_k \|Q_E f\|_{L_2} \le \text{const}.$$

Then, there exists a unique generalized solution of (34), (35), (36) satisfying the following inequality:

$$\max_t \sum_{i=1}^{3} \max_x |q_i| \le \text{const}$$

where the value of const depends only on the conditions of the theorem.

Proof. It suffices to obtain uniform estimates of the maximum velocity components q_i, which obviously follow from $\max_x |q_i|$ because uniform estimates allow us to extend the local existence and uniqueness theorem over the interval in which they are valid. To estimate the velocity components, Lemma 22 can be used:

$$v_i = q_i \Big/ \left(\int_0^T \|q_x\|^2_{L_2\left(R^3\right)}\mathrm{d}t + A_0 + 1\right), \quad A_0 = \frac{4}{\nu^{\frac{1}{3}}\left(CC_0+1\right)^{\frac{2}{3}}}.$$

Using Lemmas (25)-(29) for

$$v_i = q_i \Big/ \left(\int_0^T \|q_x\|^2_{L_2\left(R^3\right)}\mathrm{d}t + A_0 + 1\right)$$

we can obtain $\|A_i\|_{\mathrm{TA}} < \alpha < 1$ where A_i is the amplitude of potential v_i and $N(v_i) < 1$. That is, discrete solutions are not significant in proving the theorem, so its assertion follows the conditions of Theorem 6, which defines uniform time estimations for the maximum values of the velocity components.

$$\|\nabla v\|_{L_2\left(R^3\right)} + \int_0^t\int_{R^3} |\nabla v|\,\mathrm{d}k\mathrm{d}\tau \le \text{const} + \max|v|\int_0^t \|\nabla v\|_{L_2\left(R^3\right)}\left\|\nabla^2 v\right\|_{L_2\left(R^3\right)}\mathrm{d}\tau. \tag{57}$$

Theorem 6 asserts the global solvability and uniqueness of the Cauchy problem for the Navier-Stokes equations.

Theorem 7. Let

$$q_0 \in W_2^2\left(R^3\right),\ \ \nabla^2\tilde{q}_0 \in L_2\left(R^3\right),\ \ f \in L_2\left(Q_T\right),\ \ \tilde{f} \in L_1\left(Q_T\right)\cap L_2\left(R^3\right)$$

$$\lim_{t\to t_0}\left\|\nabla q\right\|_{L_2\left(R^3\right)} = \infty. \tag{58}$$

Then, there exists i, j and x_0

$$\lim_{t\to t_0}\psi_j\left(x_0,t\right) = \infty \quad \text{or} \quad \lim_{t\to t_0} N\left(q_j\right) = \infty. \tag{59}$$

Proof. A proof of this lemma can be obtained using $q_i = P_{Ac}q_i + P_D q_i$ and uniform estimates $P_{Ac}q_i$.

Theorem 7 describes the loss of smoothness of classical solutions for the Navier-Stokes equations.

Theorem 7 describes the time blow up of the classical solutions for the Navier-Stokes equations arises, and complements the results of Terence Tao [17].

4. Conclusion

New uniform global estimations of solutions of the Navier-Stokes equations indicate that the principle modeling of complex flows and related calculations can be based on the Fourier transform method.

Acknowledgements

We are grateful to the Ministry of Education and Science of the Republic of Kazakhstan for a grant, and to the System Research "'Factor" Company for combining our efforts in this project.

The work was performed as part of an international project, "Joint Kazakh-Indian studies of the influence of anthropogenic factors on atmospheric phenomena on the basis of numerical weather prediction models WRF (Weather Research and Forecasting)", commissioned by the Ministry of Education and Science of the Republic of Kazakhstan.

References

[1] Fefferman, C.L. (2006) Existence and Smoothness of the Navier-Stokes Equation. *The Millennium Prize Problems*, Clay Mathematics Institute, Cambridge, 57-67.

[2] Durmagambetov, A.A. and Fazilova, L.S. (2013) Global Estimation of the Cauchy Problem Solutions' Fourier Transform Derivatives for the Navier-Stokes Equation. *International Journal of Modern Nonlinear Theory and Application*, **2**, 232-234. http://www.scirp.org/journal/IJMNTA/

[3] Durmagambetov, A.A. and Fazilova, L.S. (2014) Global Estimation of the Cauchy Problem Solutions' the Navier-Stokes Equation. *Journal of Applied Mathematics and Physics*, **2**, 17-25. http://www.scirp.org/journal/JAMP/

[4] Durmagambetov, A.A. and Fazilova, L.S. (2014) Existence and Blowup Behavior of Global Strong Solutions Navier-Stokes. *International Journal of Engineering Science and Innovative Technology*, **3**, 679-687. http://ijesit.com/archivedescription.php?id=16

[5] Russell, J.S. (1844) Report on Wave. *Report of the Fourteenth Meeting of the British Association for the Advancement of Science*, York, Plates XLVII-LVII, 90-311.

[6] Russell, J.S. (1838) Report of the Committee on Waves. *Report of the 7th Meeting of British Association for the Advancement of Science*, John Murray, London, 417-496.

[7] Ablowitz, M.J. and Segur, H. (1981) Solitons and the Inverse Scattering Transform. *SIAM*, 435-436.

[8] Zabusky, N.J. and Kruskal, M.D. (1965) Interaction of Solitons in a Collisionless Plasma and the Recurrence of Initial States. *Physical Review Letters*, **15**, 240-243. http://dx.doi.org/10.1103/PhysRevLett.15.240

[9] Faddeev, L.D. (1974) The Inverse Problem in the Quantum Theory of Scattering II. *Itogi Nauki i Tekhniki, Seriya Sovremennye Problemy Matematiki, Fundamental'nye Napravleniya*, VINITI, Moscow, 93-180.

[10] Newton, R.G. (1979) New Result on the Inverse Scattering Problem in Three Dimensions. *Physical Review Letters*, **43**, 541-542. http://dx.doi.org/10.1103/PhysRevLett.43.541

[11] Newton, R.G. (1980) Inverse Scattering. II. Three Dimensions. *Journal of Mathematical Physics*, **21**, 1698-1715. http://dx.doi.org/10.1063/1.524637

[12] Somersalo, E., *et al*. (1988) Inverse Scattering Problem for the Schrodinger's Equation in Three Dimensions: Connections between Exact and Approximate Methods. *Journal of Mathematical Physics*, **21**, 1698-1715.

[13] Povzner, A.Y. (1953) On the Expansion of Arbitrary Functions in Characteristic Functions of the Operator. Russian, *Sbornik Mathematics*, **32**, 56-109.

[14] Birman, M.S. (1961) On the Spectrum of Singular Boundary-Value Problems. Russian, *Sbornik Mathematics*, **55**, 74-125.

[15] Poincare, H. (1910) Lecons de mecanique celeste, t. *Math. & Phys. Papers*, **4**, 141-148.

[16] Leray, J. (1934). Sur le mouvement d'un liquide visqueux emplissant l'espace. *Acta Mathematica*, **63**, 193-248. http://dx.doi.org/10.1007/BF02547354

[17] Ladyzhenskaya, O.A. (1970) Mathematics Problems of Viscous Incondensable Liquid Dynamics. Science, 288.

[18] Solonnikov, V.A. (1964) Estimates Solving Nonstationary Linearized Systems of Navier-Stokes' Equations. *Transactions Academy of Sciences USSR*, **70**, 213-317.

[19] Huang, X., Li, J. and Wang, Y. (2013) Serrin-Type Blowup Criterion for Full Compressible Navier-Stokes System. *Archive for Rational Mechanics and Analysis*, **207**, 303-316. http://dx.doi.org/10.1007/s00205-012-0577-5

[20] Tao, T. (2014) Finite Time Blowup for an Averaged Three-Dimensional Navier-Stokes Equation.

Natural Science, 2015, 7, 100-102
Published Online February 2015 in SciRes. http://www.scirp.org/journal/ns
http://dx.doi.org/10.4236/ns.2015.72011

Flow past a Groove

Kern E. Kenyon

4632 North Lane, Del Mar, USA
Email: kernken@aol.com

Received 6 February 2015; accepted 24 February 2015; published 27 February 2015

Abstract

Based on available evidence, it is hypothesized that the net force of friction on a flat solid wall, when fluid flows steadily along it, is reduced by putting one or more grooves in the wall's surface oriented perpendicular to the mean flow. Among the convincing observations are the existence and history of golf balls which show that golf balls with dimples travel farther than golf balls without dimples. Also there is a laboratory experiment using streak photography of low Reynolds number flow along a straight wall with a square cavity in it, illustrating that the flow jumps right across the cavity's opening, strongly suggesting that there is no friction of the fluid on the wall in the region of the cavity. One forecast is that if grooves or dimples are made on the inside surface of pipes, the discharged rate of the pipe for fluid flow should become increased.

Keywords

Flow past a Groove, Reduced Friction

1. Introduction

Golf balls have dimples for a good reason, which can be traced back to an accidental discovery in the mid-1800s [1]. When small scrapes or nicks occurred in the surface of the ball, observations showed that there was an increase in the distance the ball traveled. By the early 1900s, all golf balls were manufactured with dimples. Is that basically the end of the story? What is the root cause of this phenomenon? Apparently there are available no other practical applications of the idea behind the dimples of present day golf ball?

Suppose that, driven by some unspecified force, steady flow of a constant density fluid moves along a flat rigid wall and then encounters a bump in the wall. The bump's specific shape is not important, but for convenience small slopes will be assumed. Of necessity the fluid next to the bump must rise up the forward face because of the boundary condition that fluid cannot penetrate the solid surface of the bump. Then consider a steady flow along a flat rigid wall that comes to a dip (inverse bump) in the wall. There is no corresponding necessity that the fluid adjacent to the wall follow the surface downward on the front face of the dip. In general, one would not expect such a thing to happen. Note that the upward and downward directions mentioned here have nothing to

How to cite this paper: Kenyon, K.E. (2015) Flow past a Groove. *Natural Science*, **7**, 100-102.
http://dx.doi.org/10.4236/ns.2015.72011

do with the action of gravity being significant or not.

In searching through the nine fairly standard fluid dynamics books on my shelf for information on flow past a groove, I found only one text with one paragraph on the subject in it: [2]. However, on the previous page is a very interesting photograph to go with this paragraph. Streak photography was used to illustrate flow at low Reynolds number along a solid flat wall that had a square cavity in it. The depth of the cavity was comparable to its width. Assume that the flow was from left to right (the text doesn't say but the reference cited undoubtedly does [3]; it is not important for the present purpose). It is seen that the flow along the wall continues right across the opening of the cavity and then goes along the wall again on the other side of the cavity. Although not totally counter-intuitive, such an observation is just a bit surprising. Deductions that arise from this observation are given below.

2. Groove Opening

To begin with, understanding how the flow can go across the groove's opening needs to be addressed and hopefully understood better. Since the flow appears in the photograph to be steady, the streaks make the streamlines visible. Along a streamline Bernoulli's law is expected to hold approximately: where the speed is greatest the pressure is least. Thus, across the opening the pressure in the flow is lower than just below the flow in the cavity. Although it is seen in the photograph that the flow dips down a small amount at the entrance of the cavity, it is prevented from going further into the groove by the upward pressure gradient holding the flow up.

Strictly speaking Bernoulli's law is not valid when friction is involved. However, across the gap friction within the fluid is less than friction between fluid and solid along the wall because vertical velocity gradients will be less in the groove where there is no non-slip boundary condition within the opening. Also the friction term to be added to Bernoulli's law is small if the curvature of the streamlines is small [4], which it is at the groove's opening according to the streak photograph.

3. Deductions

An elementary theoretical (analytical) model of flow past a groove appears to be out of reach at present and no such model already exists as far as I can determine. Numerical techniques may be brought into service on the problem in the future, however. Of course further observations are always welcome. In the interval a few important deductions can be put forward based on the existing evidence.

First, it is self-evident from the streak photograph mentioned above that friction between the fluid and the solid wall will not only be small in the region of the groove, compared to that on the flat wall on either side of the groove, but it may actually have the opposite sign, since there appears to be a weak recirculation within the groove. In other words, at the bottom of the groove the friction force probably points upstream! Confirmation by observations of the reduction in friction by the presence of a groove is badly needed. This possible outcome of the effect of a groove on the total friction of the fluid on the wall was not mentioned in the above reference [2].

Second, if one groove reduces the net friction on the wall, even by a tiny fraction, then more grooves should reduce friction by a greater amount. For example, assuming friction reduction is their main purpose, there are about as many dimples on a golf ball as can be fitted in: well over one hundred [1].

4. Discussion

During translation through the air a golf ball almost always rotates about an axis that passes through the ball, the way the game is normally played. That introduces another force into the problem: the sideways acting Magnus effect. Then confusion can enter because the Magnus effect does have an influence on the distance the ball travels. If a golf ball can be struck without rotation, and if a ball with dimples consistently travels farther than a smooth ball, a stronger case could be made that the dimples reduce the friction between the air and the ball.

While waiting for experimental verification of the two deductions stated above about friction reduction by grooves in a solid boundary, one other application can be hazarded. Dents could be placed on the inside surface of pipes to see if the discharge rate increases. Or circular grooves could be made inside in planes parallel to vertical cross-sections of the pipe, whichever would lead to the greater result or be easier to make or both.

5. Conclusion

It is concluded that a flat solid wall experiences less friction from a fluid flowing next to it if there are one or

more grooves cut into the wall's surface in the direction normal to the mean flow. Laboratory observations strongly suggest that the conclusion is valid but further measurements are needed to confirm it. Assuming the conclusion is right, then it should also be true that a pipe will have a greater discharge rate of fluid flow when grooves are cut into the inside surface.

References

[1] Pickover, C.A. (2011) The Physics Book. Barnes & Noble, New York, 298.

[2] Tritton, D.J. (1988) Physical Fluid Dynamics. Oxford Science Publications, Clarendon Press, Oxford, 146-147.

[3] Taneda, S. (1979) Visualization of Separating Stokes Flows. *Journal of the Physical Society of Japan*, **46**, 1935-1942. http://dx.doi.org/10.1143/JPSJ.46.1935

[4] Milne-Thomson, L.M. (1955) Theoretical Hydrodynamics. 3rd Edition, Macmillan, New York, 571-572.

Call for Papers

Natural Science

A Journal Published by Scientific Research Publishing, USA
www.scirp.org/journal/ns

Editor-in-Chief

Editorial Advisory Board

Editorial Board

Natural Science is an international journal dedicated to the latest advancement of natural sciences. The goal of this journal is to provide a platform for scientists and academicians all over the world to promote, share, and discuss various new issues and developments in different areas of natural sciences. All manuscripts must be prepared in English, and are subject to a rigorous and fair peer-review process. Accepted papers will immediately appear online followed by printed hard copy. The journal publishes original papers including but not limited to the following fields:

- **Astronomy & Space Sciences**
  - Astronomy
  - Astrophysics
  - Atmospheric Science
  - Space Physics
- **Earth Science**
  - Geography
  - Geology
  - Geophysics/Geochemistry
  - Oceanography
- **Chemistry**
  - Analytical Chemistry
  - Biochemistry
  - Computational Chemistry
  - Inorganic Chemistry
  - Organic Chemistry
  - Physical Chemistry
- **Life Science**
  - Cell Biology
  - Computational Biology
  - Genetics
  - Immunology
  - Medicine/Diseases
  - Microbiology
  - Molecular Biology
  - Neuroscience
  - Pharmacology/Toxicology
  - Physiology
  - Psychology
  - Virology
- **Physics**
  - Applied Physics
  - Atomic, Molecular, and Optical Physics
  - Biophysics
  - High Energy/Particle Physics
  - Material Science
  - Plasma Physics
- **Others**
  - Education
  - History of Science
  - Science and Innovations

We are also interested in: 1) Short Reports—2-5 page papers where an author can either present an idea with theoretical background but has not yet completed the research needed for a complete paper or preliminary data; 2) Book Reviews—Comments and critiques.

Notes for Intending Authors

Submitted papers should not be previously published nor be currently under consideration for publication elsewhere. Paper submission will be handled electronically through the website. For more details, please access the website.

Website and E-Mail

http://www.scirp.org/journal/ns E-mail: ns@scirp.org

What is SCIRP?

Scientific Research Publishing (SCIRP) is one of the largest Open Access journal publishers. It is currently publishing more than 200 open access, online, peer-reviewed journals covering a wide range of academic disciplines. SCIRP serves the worldwide academic communities and contributes to the progress and application of science with its publication.

What is Open Access?

All original research papers published by SCIRP are made freely and permanently accessible online immediately upon publication. To be able to provide open access journals, SCIRP defrays operation costs from authors and subscription charges only for its printed version. Open access publishing allows an immediate, worldwide, barrier-free, open access to the full text of research papers, which is in the best interests of the scientific community.

- High visibility for maximum global exposure with open access publishing model
- Rigorous peer review of research papers
- Prompt faster publication with less cost
- Guaranteed targeted, multidisciplinary audience

Scientific Research Publishing

Website: http://www.scirp.org

Subscription: sub@scirp.org

Advertisement: service@scirp.org